Cell Systems

Engineered Fluorescent *E. coli* Lysogens Allow Live-Cell Imaging of Functional Prophage Induction Triggered inside Macrophages

Graphical Abstract

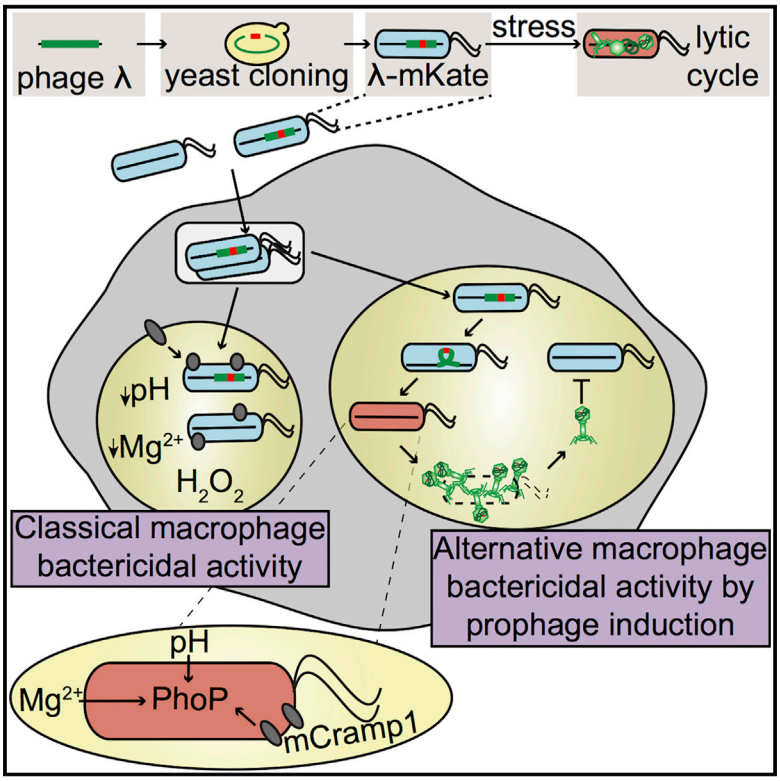

Highlights

- A bacteriophage lysis reporter allows for live-cell imaging of prophage induction
- Macrophages trigger λ phage induction and lysis in phagocytosed *E. coli* through PhoP
- Induced λ phage can propagate secondary *E. coli* infections inside phagosomes

Authors

Katie Bodner, Arin L. Melkonian, Angela I.M. Barth, Takamasa Kudo, Yu Tanouchi, Markus W. Covert

Correspondence

mcovert@stanford.edu

In Brief

The immune system encounters many bacteria that are infected with dormant viruses (phages) that have the potential to "reawaken" and lyse their host. To observe the nature of these interactions, we set up a platform to image the phage λ with a fluorescent reporter for lysis inside *E. coli* engulfed by macrophages. We visualized macrophages triggering internalized *E. coli* to induce λ and lyse. Induced particles can kill neighboring bacteria, demonstrating that phages provide an alternative bacterial killing pathway for macrophages.

Bodner et al., 2020, Cell Systems *10*, 254–264
March 25, 2020
https://doi.org/10.1016/j.cels.2020.02.006

CellPress

CellPress

Cell Systems
Report

Engineered Fluorescent *E. coli* Lysogens Allow Live-Cell Imaging of Functional Prophage Induction Triggered inside Macrophages

Katie Bodner,[1,2] Arin L. Melkonian,[1,2] Angela I.M. Barth,[1,2,5] Takamasa Kudo,[2,3] Yu Tanouchi,[1,2,4] and Markus W. Covert[1,2,6,*]

[1]Department of Bioengineering, Stanford University, Stanford, CA 94305, USA
[2]Allen Discovery Center for Systems Modeling of Infection, Stanford University, Stanford, CA 94305, USA
[3]Department of Chemical and Systems Biology, Stanford University, Stanford, CA 94305, USA
[4]Present address: X, formerly Google X, 100 Mayfield Ave, Mountain View, CA 94043, USA
[5]Present address: Department of Pediatrics, Stanford University, Stanford, CA 94305, USA
[6]Lead Contact
*Correspondence: mcovert@stanford.edu
https://doi.org/10.1016/j.cels.2020.02.006

SUMMARY

Half of the bacteria in the human gut microbiome are lysogens containing integrated prophages, which may activate in stressful immune environments. Although lysogens are likely to be phagocytosed by macrophages, whether prophage activation occurs or influences the outcome of bacterial infection remains unexplored. To study the dynamics of bacteria-phage interactions in living cells—in particular, the macrophage-triggered induction and lysis of dormant prophages in the phagosome—we adopted a tripartite system where murine macrophages engulf *E. coli*, which are lysogenic with an engineered bacteriophage λ, containing a fluorescent lysis reporter. Pre-induced prophages are capable of lysing the host bacterium and propagating infection to neighboring bacteria in the same phagosome. A non-canonical pathway, mediated by PhoP, is involved with the native λ phage induction inside phagocytosed *E. coli*. These findings suggest two possible mechanisms by which induced prophages may function to aid the bactericidal activity of macrophages.

INTRODUCTION

Although bacteriophages are the most abundant organisms on Earth, their direct impact on human health and disease remains to be fully appreciated (reviewed in Barr, 2017; Keen and Dantas, 2018; Mirzaei and Maurice, 2017). A frontier of particular interest concerns how bacteriophages influence the bactericidal mechanism of mammalian cells (reviewed in Van Belleghem et al., 2018). Bacteriophages can be engulfed by macrophages through phagocytosis, and once internalized by dendritic cells they have been shown to indirectly promote dampened phagocytosis of a bacterial pathogen (Hodyra-Stefaniak et al., 2015; Sweere et al., 2019). Though these prior studies are compelling, they required the addition of either inflammatory pre-stimulation or delivery of a large population of phage to produce their effects. Thus, the physiological significance of direct phage-human interactions is only beginning to be delineated.

Prior work suggests that one possible mechanism of bactericidal activity of bacteriophages in macrophages occurs through a bacterial intermediate. If a bacterial lysogen carrying a prophage induces the lytic state before or during phagocytosis, the resulting prophage may have the ability to kill the host bacterium (first postulated in Skurnik and Strauch, 2006). Prophage induction has been observed in bone-marrow-derived macrophages infected with lysogenic *Listeria monocytogenes*, leading to the excision of phage DNA; however, neither bacterial cell lysis nor functional phage particles were detected inside the macrophages (Rabinovich et al., 2012). Studies of live mice treated with lysogenic bacteria and then assayed for bulk phage particles within the feces have confirmed that lysogens can produce phage particles *in vivo*, possibly due to inflammation in the gut (De Paepe et al., 2016; Oh et al., 2019; Diard et al., 2017), but how or where these particles were produced was not established. As a result, major questions remain unanswered about whether functional prophages can be produced in the mammalian host cell and what environmental cues inside phagosomes specifically trigger prophage induction.

To observe how prophages influence bacterial killing by immune cells, one relevant experimental model would be tripartite: the simultaneous observation of bacteriophages within host bacteria, which have been engulfed by phagocytic cells. The events surrounding infection in such a tripartite system would evolve in complex ways over time and differently in individual immune cells—meaning that interrogation of this system would require dynamic measurement techniques, single-cell resolution, and fine perturbation approaches. In contrast, the primary means for assessing a phage population have been either sequence based (Manrique et al., 2016) or assaying for bulk phage particles via plaque assay—both of which preclude tracking of distinct bacteriophage populations in specific cell types over time. Genetic perturbation of phages has also been notoriously difficult to engineer, due in particular to their large genome sizes, the need for multiple genetic markers, and a prohibitively low yield (reviewed in Pires et al., 2016). A major step

forward in phage engineering occurred when yeast recombination techniques were used to modify lytic phages (Ando et al., 2015); however, this technique requires several adaptations before it can be applied to lysogenic phages, with their dual life cycle and multiple genomic orientations.

Here, we describe the engineering of various selection markers and fluorescent proteins into bacteriophage λ using a lysogenic phage-specific modification of the Ando et al. (2015) protocol. As a result, our tripartite system is highly amenable to high-throughput, live-cell imaging, allowing us to witness prophage induction state in real time in individual bacteria. We observed functional induction and lysis in a substantial population of bacterial-infected macrophages. Our ability to capture the single-cell heterogeneity in these infections revealed that prophages tend to induce more frequently from bacteria that remain in the macrophage for several hours. This led us to postulate and identify a pathway for bacterial lysis induced by macrophages, involving the *E. coli* transcriptional regulator, PhoP, a sensor of environmental stress including low Mg^{2+}, antimicrobial peptides (AMPs), and acidic pH. Single-cell resolution also enabled us to witness very rare events including an alternate pathway of bactericidal activity, the transfer and propagation of functional phage particles between bacterial strains in the phagosome. Thus, macrophage-generated stress on phagocytosed bacteria appears to play multiple roles in bacterial killing via prophage induction.

RESULTS

A Bacteriophage Lysis Fluorescent Reporter Allows for the Study of Prophage Induction in Real Time

We chose to engineer the most well-characterized *E. coli* phage, bacteriophage λ, to contain a fluorescent reporter in the lysis operon. The lysogenic phage-specific modifications to the Ando et al. (2015) protocol are detailed in the STAR Methods and highlighted in Figure 1A. We designed the λ lysis reporter to include the fluorescent protein, mKate2, in the late-lysis operon with its own ribosomal binding site (as opposed to a coat protein fusion design, which may influence titer; Trinh et al., 2017) replacing several non-essential genes in order to retain the final phage genome at a size of ~48.1 kb, for efficient capsid packaging (Figure 1B). The late-lysis operon stays repressed while the prophage is integrated. When prophage induction occurs, the genome excises, replicates, and begins to express early- and late-lysis genes, which should be concurrent with expression of the mKate2, allowing us to monitor prophage induction in real time.

We validated the reporter phage (hereby λ mKate) by live-cell imaging on an agar pad to test reporter function as a readout for prophage induction. We tested both the λ mKate lysogen, as well as a lysogen with a temperature-sensitive mutant of the λ repressor cI. The temperature-sensitive mutant, *cI857*, denatures at 42°C, leading to de-repression of lysis genes and prophage induction (Lieb, 1966). We applied a DNA-damaging antibiotic, norfloxacin (NFX), to the wild type (WT), which should trigger the main pathway used by *E. coli* for prophage induction, the RecA-mediated SOS response (Matsushiro et al., 1999). For the *cI857*, we applied a 15-min 42°C heat shock prior to imaging (Figure 1C). At the beginning of the time course, there was no notable expression of the mKate reporter in the *cI857* strain (Figure 1D). The frequency of induction then rose to a maximum of 5.8×10^{-1} at 3 h post-heat shock (Figure 1E; *cI*857 HS) and 1.8×10^{-3} without heat shock (Figure 1E; *cI857* Unstim), and many of the inducing bacteria lysed (Figure 1D, white arrows; Video S1). To determine how accurately the reporter reflects phage lysis events, we quantified the fraction of bacteria expressing mKate with respect to the population that lyses, which was 89.2% ± 4.8% (Figure S1C). For the uninduced λ mKate, the frequency of bacteria expressing the reporter plateaus at 7.7×10^{-3} (Figure 1E; *cI* WT Unstim; Video S2). If the λ mKate lysogen is pre-stimulated with NFX, the frequency of prophage induction with the reporter significantly ($p = 0.033$) rises to 1.7×10^{-2} before 6 h post-stimulation (Figures 1E; *cI* WT NFX and S1D; Video S3). Compared with another mKate phage we constructed without the non-essential gene deletions, λ mKate did not differ in spontaneous induction frequency after close to 6 h growth (Figures S1E and S1F, $p = 0.83$). Finally, λ mKate showed slight defects in infectivity in bulk culture—a 1.17 h delay in lysis timing ($p = 0.00012$) and a 2.17 h delay in re-lysogenization ($p = 0.0003$); however, this phage still lysed a culture of *E. coli* to 13.1% of peak optical density (OD) (Figure S1G). We concluded that λ mKate is functional and can serve as an accurate readout of phage induction state.

Macrophages Actively Trigger Prophage Induction in Phagocytosed *E. coli*, which Promotes Increased Bacterial Clearance

After validating the induction reporter *in vitro*, we asked whether prophage induction occurs when *E. coli* lysogens are phagocytosed. We infected murine RAW264.7 cells (a macrophage-like cell line) with the λ mKate lysogen and monitored induction through reporter expression over time. Along with the prophage reporter, we used a lab strain of *E. coli* MG1655 that constitutively expresses the fluorescent protein mCerulean3 from a low copy plasmid. RAW264.7 cells also contained a H2B-miRFP670 nuclear marker (see STAR Methods) to facilitate cell image analysis (Figures 2A and S3). Using this system, we observed bacterial cells inside the macrophage phagosome undergoing phage induction and lysis, as indicated by the change in bacterial morphology from filamentous to round at 18 h and the loss of phage reporter signal at 21 h post-infection (Figures 2B and 2C; Video S4). The mean phage reporter signal stayed below 3% maximal activation until the bacteria were phagocytosed for more than 10 h (example shown in Figure 2C). Bacteriophage induction occurred in late stages of the infection, as 87% of the peak intensities happened later than 10 h post-infection (Figure 2D). By 21 h post-infection, prophage induction had occurred in ~20% of macrophage cells infected with bacteria (Figure 2E).

Bacteriophage lysis events were also characterized by a disappearance of phage reporter prior to loss of the bacterial reporter signal (Figure 2B). The delayed clearance of released bacterial protein is most likely due to differences in either reporter protein expression levels (the bacterial reporter is expressed from a synthetic promoter on a plasmid whereas the phage reporter is part of a lysis transcript) or acid stability of the reporters in the phagosome (Cranfill et al., 2016). As supporting evidence that the bacteria within the phagosome have lysed, we also observed a similar morphology change and phage reporter

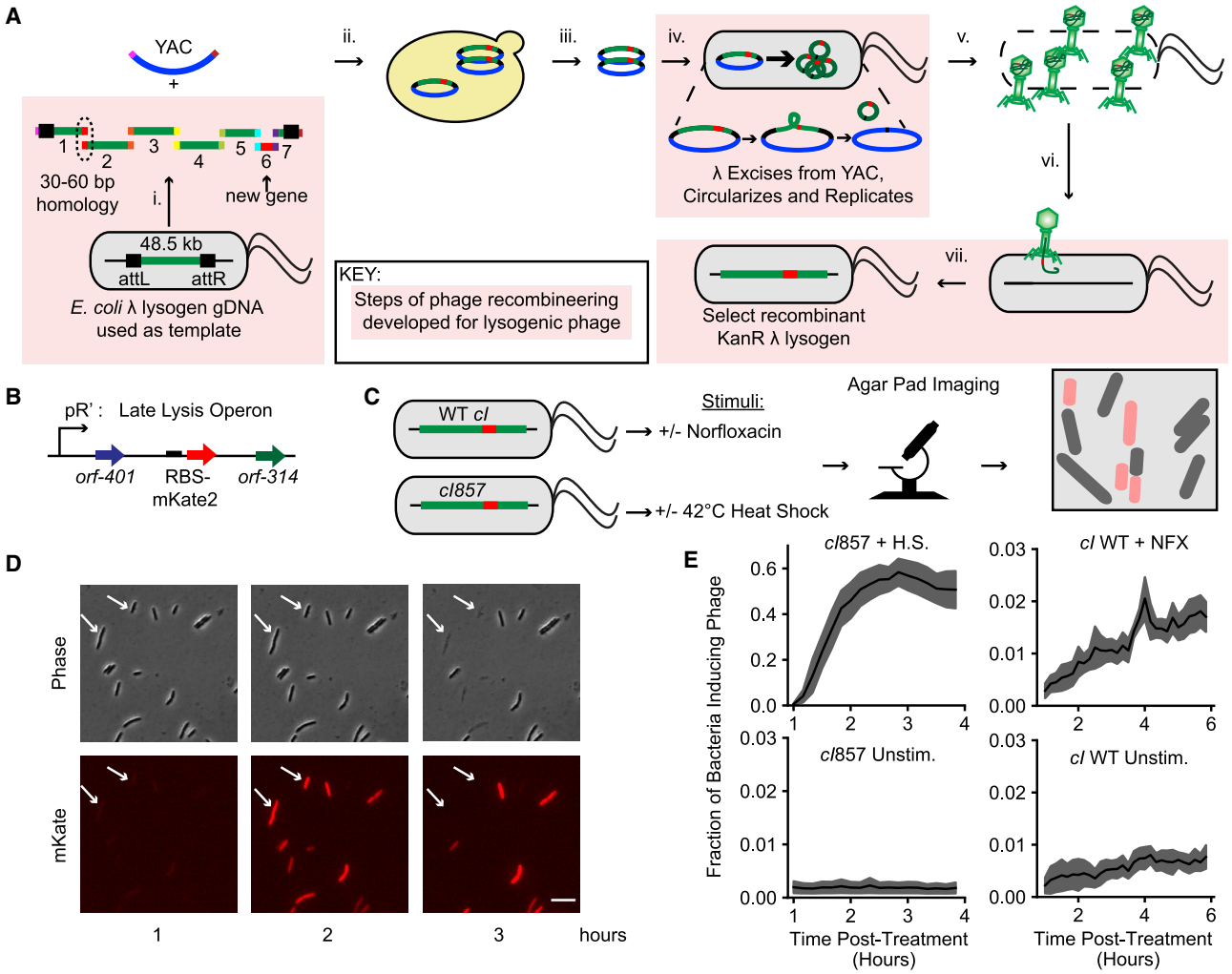

Figure 1. A Yeast Recombination Strategy Enables Rapid Construction and Testing of a Synthetic λ Phage with a Lysis Reporter

(A) The yeast recombination workflow for multiplexing modifications to the λ phage genome. Boxes in pink indicate workflow steps specifically modified from Ando et al. (2015) for cloning lysogenic phage. (Ai) The λ genome was used as a PCR template in the genomic DNA configuration. (Aii) The PCR products and yeast artificial chromosome (YAC) were transformed into yeast. (Aiii) Yeast colonies were screened for correct assembly by colony PCR (Figures S1A and S1B), and the total genomic DNA (gDNA) was extracted. (Aiv) The gDNA was electroporated into non-lysogenic *E. coli*. (Av) The replicating phage DNA packaged into particles, which (Avi) infected another non-lysogenic *E. coli* strain. (Avii) *E. coli* recombinant lysogens were isolated by kanamycin selection.

(B) The design of the lysis reporter. A synthetic RBS and mKate2 were inserted between *orf*-401 and *orf*-314, genes lowly expressed during lysis (Liu et al., 2013). The pR′ promoter, active during late phage lysis, drives mKate2 expression.

(C) The experimental design for validating the lysis reporter of λ mKate. MG1655 *E. coli* carrying the WT *cI* or *cI857* λ mutant were stimulated with either a DNA-damaging antibiotic (NFX) or a heat shock, respectively. Lysogens were spotted onto an agar pad and imaged for 3–5 h post-stimulation at 37°C in the Phase and mKate channels.

(D) Still images from the time course of λ mKate (*cI857*) post-heat shock. The mKate channel shows activation of the late-lysis mKate2 reporter. White arrows indicate cells that undergo activation of the mKate reporter followed by bacterial lysis. Scale bar, 10 μm.

(E) The average fraction of bacteria expressing the lysis reporter. For *cI857*, n = 3 independent experiments were analyzed from a total of four positions per strain with a total of 2,451 cells for the heat-shock condition and 5,962 cells for untreated. For *cI* WT, the frequency was calculated for uninduced versus induced bacteria with 50 ng/mL NFX for 30 min prior to imaging. n = 5 independent experiments were performed, and images were analyzed from a total of 14 frames. 11,942 cells for unstimulated and 12,365 for NFX. Shaded regions are ± 1 SEM. At the final time point, a significantly higher fraction of the NFX-stimulated *cI* WT *E. coli* induced than the unstimulated ($p = 0.033$).

See also Figure S1; Videos S1, S2, and S3; Table S1.

disappearance in successful phage lysis events inside of macrophages with the heat-shocked mKate *cI857* lysogen (Figures S2A and S2B).

Subsequently, we wanted to compare the frequency of prophage induction within macrophages with respect to frequencies that had previously been measured outside of macrophages, for example, *in vitro* on agar pads. By estimating the number of inducing bacteria per macrophage from the imaging data (Figures S2C–S2G; STAR Methods: Bounds analysis for bacterial prophage induction frequency inside macrophages),

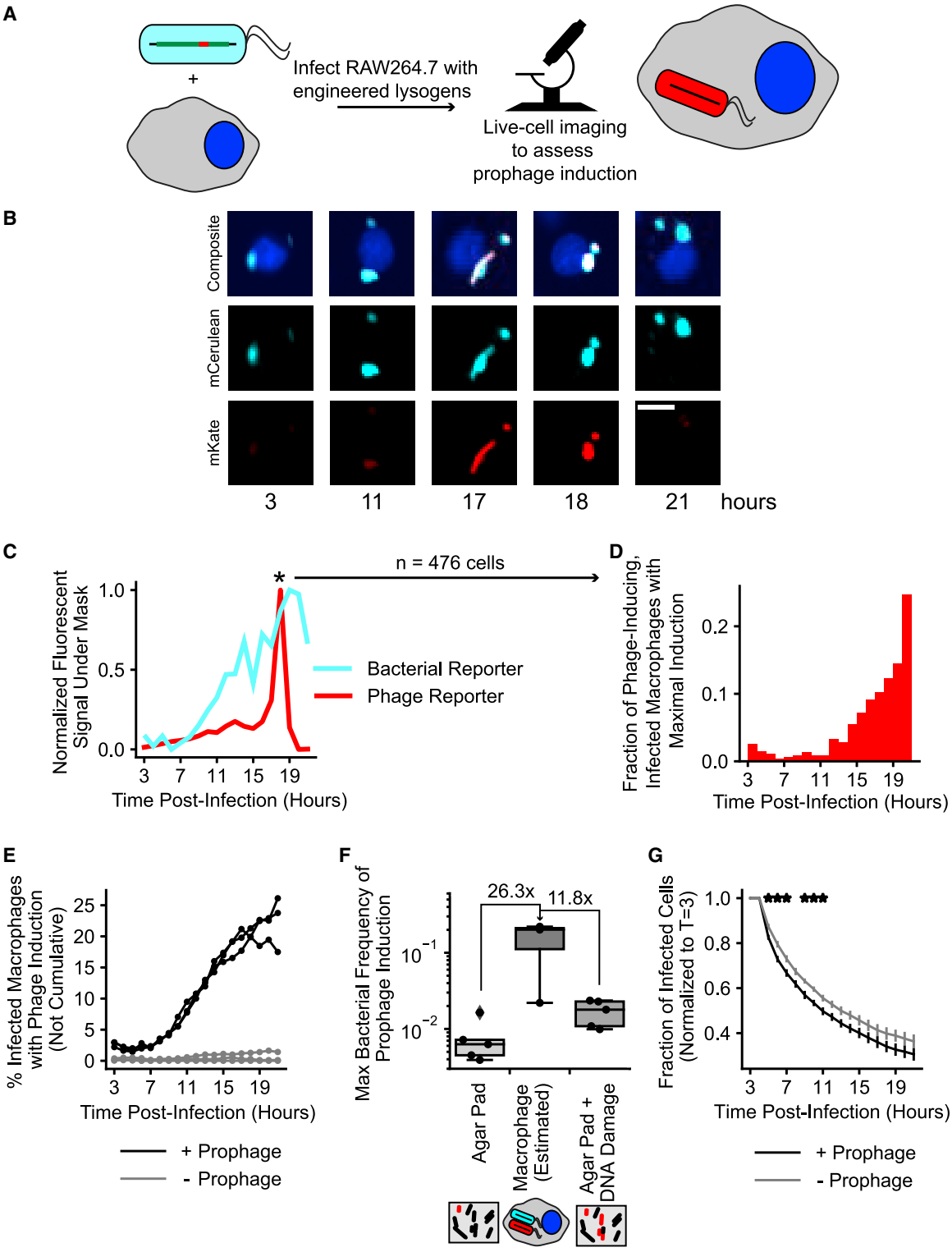

Figure 2. Monitoring of Prophage Induction with a Lysis Reporter Reveals More Frequent Prophage Induction in Bacteria Phagocytosed by Macrophages and Increased Clearance of Phagocytosed Lysogenic Compared to Non-lysogenic Bacteria

(A) Engineered *E. coli* λ mKate lysogens (WT *cI*) were infected at multiplicity of infection (MOI) 10 into RAW264.7 macrophages with H2B-miRFP670 nuclear marker. Lysogens also contain a constitutive mCerulean3 plasmid as a bacterial cell marker. Prophage induction in phagocytosed bacteria was recorded every hour for 21 h starting 3 h after infection.

(legend continued on next page)

we approximated a range of prophage induction frequencies between 2.2×10^{-2} and 2.2×10^{-1} bacteria (Figure 2F). This corresponds to a mean frequency that is 26-fold more frequent than unstimulated bacteria on an agar pad, and 11-fold more frequent than bacteria stimulated with NFX (Figures 2F and S2G). We confirmed that neither the components of the DMEM media, a secreted factor from the RAW264.7 cells in conditioned media, nor the antibiotic gentamicin added to the media during infection induces prophage induction significantly over basal levels (Figure S2H). These results suggest that the induction events are not spontaneous but rather that an active trigger within the macrophage intracellular environment promotes bacteriophage induction.

Next, we considered how the frequency of prophage induction observed in phagocytosed *E. coli* impacts macrophage ability to kill bacteria. We infected RAW264.7 cells with either non-lysogenic or with λ mKate lysogenic *E. coli* and tracked the fraction of cells that were able to clear the bacteria. At every time point, a higher fraction of the macrophages infected with non-lysogenic bacteria remained infected, as compared with the cells infected with a lysogenic strain (Figure 2G), in particular during the first 10 h. Both strains have nearly identical growth rates *in vitro* (Figure S2I, $p > 0.05$), suggesting that the probable cause for better clearance by macrophages is not a growth deficiency of the lysogenic strain. To the contrary, it appears that bacterial prophage carriage leads to different clearance outcomes for macrophages.

PhoP Sensing of Phagosomal Stress Factors Is Responsible for Prophage Induction inside Live Macrophage Cells

For macrophages to utilize bacteriophages for bacterial killing, we postulated that there must be a stress signal delivered to the phagosomes and considered which *E. coli* stress response pathways could sense phagosomal stress (Figure S4A). The canonical stress pathway for λ induction in *E. coli* is the RecA-dependent SOS response, which repairs DNA damage in response to antibiotics and hydrogen peroxide (H_2O_2) and also cleaves the λ repressor, leading directly to induction (reviewed in Nanda et al., 2015). Alternate prophage induction pathway candidates include the gene *rcsA*, which functions to counteract AMPs, osmotic shock, and low pH-induced membrane damage (Rozanov et al., 1998, reviewed in Majdalani and Gottesman, 2005), and PhoP, which helps *E. coli* adapt to low-magnesium environments and resist acid stress and AMPs (Monsieurs et al., 2005; Alteri et al., 2011)—although the environmental conditions that stimulate induction through these pathways remain uncharacterized. We assessed whether these pathways were involved in inducing λ mKate in *E. coli* in the phagosome by lysogenizing the Δ*recA*, Δ*phoP*, and Δ*rcsA* strains from the Keio collection (Baba et al., 2006) with λ mKate. We also tested an additional strain deficient in GadB, a glutamate decarboxylase enzyme that consumes H^+ to help bacteria survive acidic conditions but has no association with prophage induction (Gut et al., 2006).

We compared each single-gene knockout mutant to the BW25113 parent strain from the Keio collection, hereby referred to as WT (Baba et al., 2006). RAW264.7 cells were infected with either the lysogenic WT or Δ*recA*, Δ*phoP*, Δ*rcsA*, or Δ*gadB* strains and imaged for 18 consecutive h to assess the role these pathways play in prophage induction *in vitro* cell culture (Figure 3A). We found that WT *E. coli* experienced prophage induction in 6.3% of the initial infected macrophage population by the end of the infection (Figures 3Bi and 3Ci). The Δ*recA* mutant experienced prophage induction in 12.9% of all bacterial-infected RAW264.7 cells by 21 h post-infection (Figure 3Ci), which was significantly higher than WT. We also observed that the Δ*gadB* and Δ*rcsA* strains did not significantly differ from WT levels of induction (Figures 3Bi and 3Ci). Of the tested *E. coli* strains, only Δ*phoP* displayed a strong reduction in prophage induction *in vitro* cell culture, inducing in only 1.43% of infected macrophages, ~4.5-fold lower than WT by 21 h post-infection (Figures 3Bi and 3Ci).

However, we also observed that the Δ*phoP* mutant has a much reduced viability in macrophage cells due to its deficiency in resisting acid stress and Mg^{2+} starvation: we observed that only 10.8% of the initially infected RAW cells still maintained Δ*phoP* lysogens at 21 h post-infection, whereas for WT, this was 26% (no other mutant showed a significant difference in clearance, see Figure S4B). To account for this difference, we re-analyzed the data from Figures 3Bi and 3Ci, including only

(B) An example macrophage with a phagocytosed bacterium that undergoes prophage induction and lysis. Upper panel is an overlay of nuclear marker H2B-miRFP670 (blue), bacterial marker mCerulean3 (light blue), and phage lysis marker mKate (red). Middle panel is bacterial marker only. Bottom panel is phage marker only. Scale bar, 10 μm.

(C) Time series trace from the cell in (B). In light blue (——), the normalized total bacterial signal, and in red (——), the normalized mean phage signal over time. Fluorescence intensity under bacterial or phage masks was normalized to the lowest and highest intensity for each.

(D) RAW264.7 cells were tracked for 18 h, starting 3 h after infection, and phage lysis reporter signal was determined as in (C). For cells (n = 476) that had phage induction lasting at least 3 h, the time point at which phage reporter signal was at its maximum was plotted in a histogram for all cells analyzed across n = 3 independent experiments.

(E) Percentage of bacterial-infected macrophages with at least one bacterium expressing the prophage induction reporter was measured at each time point, individually. In black (——), + Prophage indicates macrophages (n = 11,793 cells) infected with lysogens, and in light gray (——), −Prophage indicates macrophages (n = 11,898 cells) infected with non-lysogen controls to validate phage reporter detection limit. Each curve is from an independent experiment.

(F) Estimation of bounds on prophage induction frequency inside macrophages is compared with frequency on an agar pad. The frequency of phage induction across all environmental contexts is defined as the number of phage-reporter-positive bacterial cells of the total bacterial cells imaged at a time point. For the macrophage condition, the estimated best frequency of induction from Figure S2G is the median, and the two whiskers are the theoretical best- and worse-case bounds estimated in STAR Methods. 3,751 macrophages were assessed across three independent experiments. The agar pad bars are re-plotted from the maximal frequency time point, T = 5.83 h, Figure 1E for the *cI* WT unstimulated and NFX conditions (n = 5).

(G) Macrophages infected with bacteria were tracked over time, and bacterial clearance was determined from disappearance of a detected bacterial mask from the cell for at least 3 consecutive h. The fraction of total infected macrophages was plotted for the lysogen (+ Prophage, 5,742 cells) and non-lysogen (− Prophage, 5,235 cells). Lines are averages ± 1 SEM from n = 4 independent experiments. * is above time points ($p < 0.05$) by Student's two-sided t test.

See also Figures S2 and S3; Video S4.

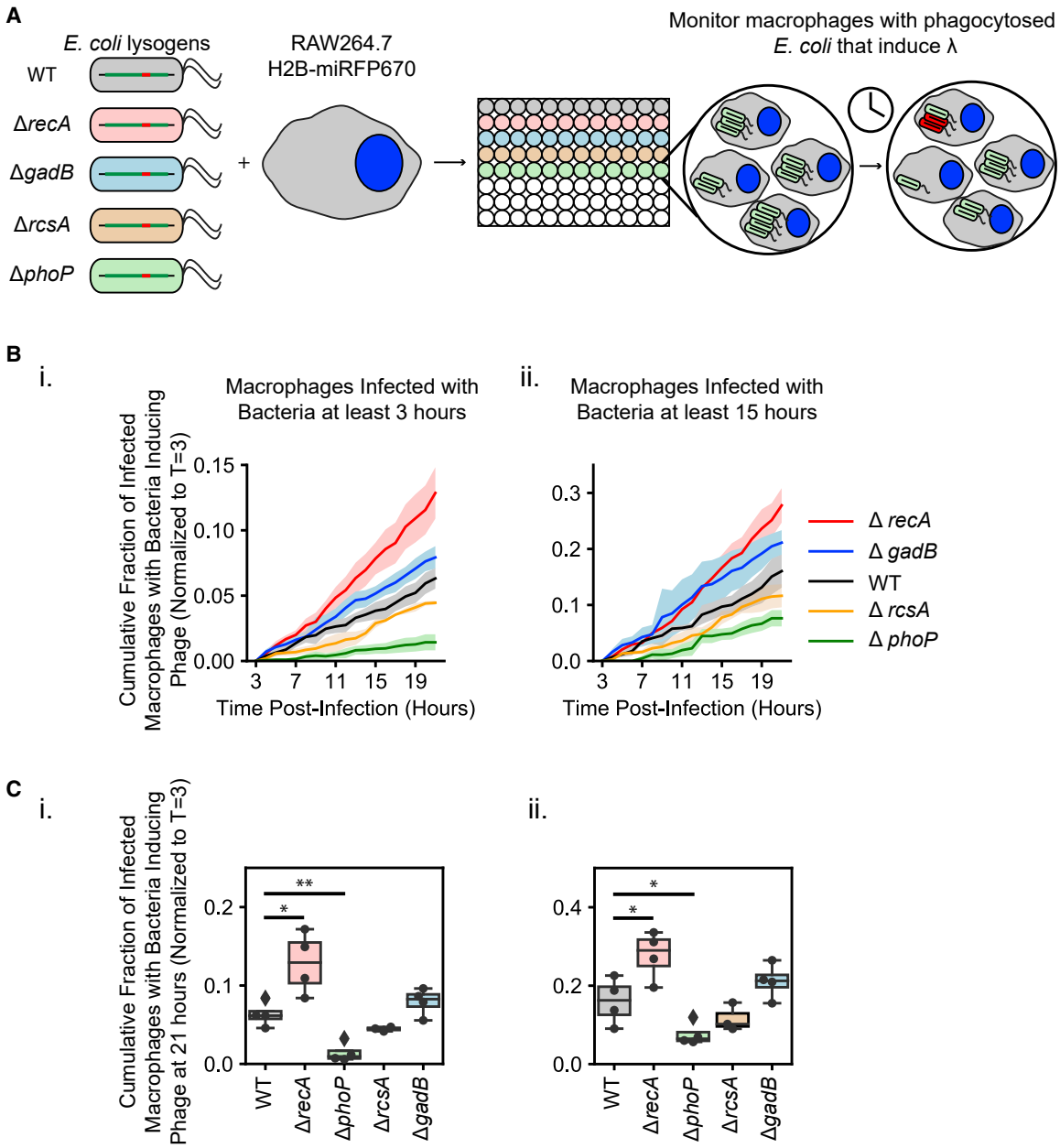

Figure 3. PhoP Sensing of Phagosomal Stress, and Not the Canonical RecA, Is Responsible for Prophage Induction inside Live Macrophage Cells

(A) Overview of experimental workflow to test prophage induction frequency of macrophage- phagocytosed *E. coli* stress-sensing mutants.

(B) Prophage induction comparison of phagocytosed *E. coli* knockouts versus WT inside macrophages. For image analysis details, see Figure S3 and STAR Methods. The y axis is the cumulative fraction of infected macrophages that have at least one phage induction event throughout the time course. The fractions are normalized by setting the values for 3 h post-infection to zero. Infected cells are considered to be those that track with bacteria consecutively for the (Bi) first 3 h of the time lapse (equivalent to h 3–6 post-infection) or (Bii) first 15 h of infection (equivalent to h 3–18 post-infection), to control for macrophage populations with slow bacterial clearance. Each curve is the average of n = 4 experiments for WT (n = 3,852 cells tracked total), Δ*recA* (n = 3,086 cells tracked total), Δ*gadB* (n = 3,642 cells tracked total), Δ*phoP* (n = 3,472 cells tracked total), and n = 3 experiments for Δ*rcsA* (n = 2,581 cells tracked total). The shaded regions are ± 1 SEM.

(Ci) The cumulative fraction from (Bi) at 21 h post-infection. WT versus Δ*phoP*: p = 0.0027; WT versus Δ*recA*: p = 0.022; WT versus Δ*rcsA*: p = 0.16; WT versus Δ*gadB*: p = 0.22. (Cii) The cumulative fraction from (Bii) at 21 h post-infection. WT versus Δ*phoP*: p = 0.043; WT versus Δ*recA*: p = 0.033; WT versus Δ*rcsA*: p = 0.56; WT versus Δ*gadB*: p = 0.22 (*p < 0.05, **p < 0.005, by Student's two-sided t test).

See also Figures S3 and S4; Table S1B.

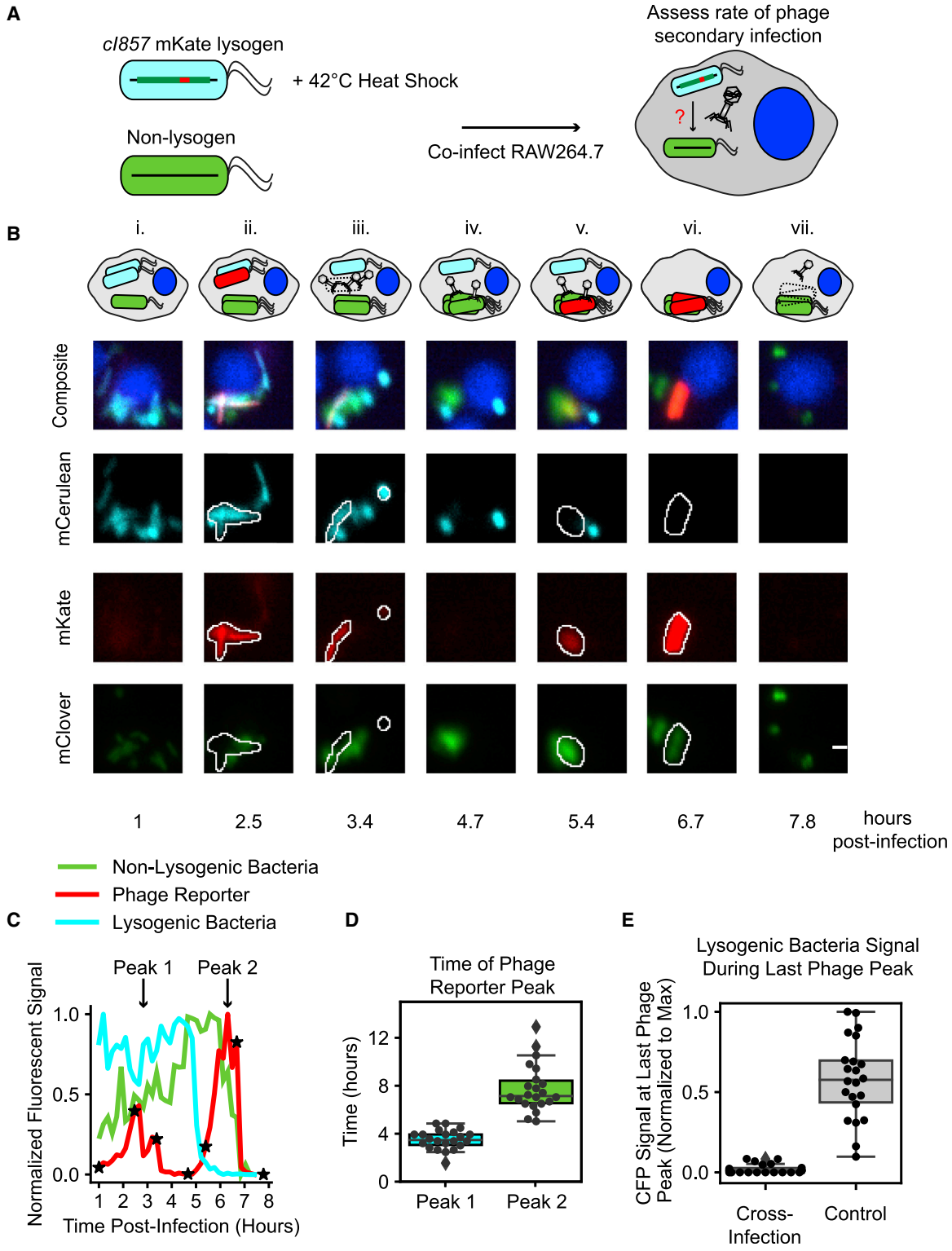

Figure 4. Induced Phage Particles Produce a Secondary Infection in a Co-infecting Bacterium

(A) Experimental design to observe bacteriophage cross-infection inside macrophages. RAW264.7 H2B-miRFP670 cells were co-infected with two bacterial strains at a total MOI of 30. *E. coli* λ mKate lysogens (*cI857*) with constitutive mCerulean3 were heat shocked for 15 min at 42°C prior to co-infection. The second strain was a recipient, non-lysogenic *E. coli* containing a constitutive mClover expression plasmid. The cells were imaged starting 1 h post-infection for 14 h every 11 min.

(legend continued on next page)

the macrophages in which the *E. coli* infection was maintained for at least 15 h without clearance. In this analysis, Δ*phoP* still induces significantly less than WT, 7.6% versus 16% of infected macrophages by 21 h post-infection (Figures 3Bii and 3Cii). These results confirm that the difference in prophage induction between the WT and Δ*phoP* lysogenic strains cannot be explained by clearance alone.

In basal growth conditions, the Δ*phoP* mutant did not display a significant defect in induction frequency from the WT (Figure S4C), so we identified a set of environmental factors within phagosomes that also stimulate PhoP, which we then cross-referenced to determine if they could also be sensed by *E. coli* and lead to bacteriophage induction. This set included acidic pH, depleted Mg^{2+} and AMPs, all previously implicated in prophage induction *in vitro* in various species of phage (Figure S4A; Flannagan et al., 2009; Imamovic and Muniesa, 2012; Nanda et al., 2015; Madera et al., 2009). In a low-pH medium (see STAR Methods), the Δ*phoP* mutant was reduced >4-fold in induction frequency as compared with WT, whereas the Δ*recA E. coli* lysogen was not significantly different (Figure S4D). When grown in Mg^{2+}-reduced medium, Δ*phoP* and Δ*recA* both induced at a significantly lower frequency than WT (Figure S4E). Finally, we tested the AMP mCramp1, a homolog of the human cathelicidin used to permeabilize the inner membrane of bacteria, which is also a murine macrophage-produced AMP known to stimulate both RcsA and PhoP (Gallo et al, 1997; Farris et al., 2010). Prophage induction in mCramp1-supplemented medium was 10-fold lower in Δ*phoP* than in WT *E. coli*, 2-fold lower in Δ*rcsA*, and roughly 1.5-fold higher in Δ*recA* (Figure S4F). The mCramp1 peptide enhanced induction over spontaneous frequencies, as we observed a modest yet significant induction increase with WT and Δ*recA* lysogens yet no significant change with stimulated Δ*rcsA*- and Δ*phoP*-lysogens (Figure S4G). These results indicate that PhoP, in a RecA-independent manner, is required for mCramp1-mediated prophage induction and suggest that a mammalian-produced AMP can induce dormant prophage.

Induced Phage Particles in the Phagosome Produce a Secondary Infection Capable of Lysing a Co-infecting Bacterium

If activated prophages are capable of forming functional particles, we postulated that another mechanism of bactericidal activity inside macrophages could be the propagation of infection and lysis to other bacteria. We developed a two-strain, donor-and-recipient infection strategy to examine whether a secondary infection could occur in the phagosome environment (Figure 4A). The phage donor strain of *E. coli*, labeled with mCerulean3, also harbored a temperature-sensitive λ mKate (*cI857*) lysogenic prophage, whereas the recipient strain, labeled with mClover, was a non-lysogen. We chose the *cI857* mutant for the donor lysogen in the co-infection experiments to maximize the conditions for observing a secondary infection: in a control population infected with the λ mKate (*cI857*) lysogen, at maximum, ~55% of infected RAW264.7 macrophages contained lysogens that were inducing by 3 h post-infection (Figure S4I). Incidentally, this timing is similar to when the maximal fraction of heat-shocked *cI857* lysogens activates *in vitro* (Figure 1E), suggesting that when induction begins just before macrophage infection, the kinetics of phage induction are not slowed down.

Using live-cell imaging, we were able to identify and track the 44% of macrophages that were infected with both a donor and a recipient (Figure S4J). In this population, we identified "cross-infection events" in which the donor strain in a given macrophage induced expression of phage genes and lysed—and then, at a later time point, a recipient bacterium in close proximity also expressed phage genes and lysed (Figure 4B; see also Video S5). We observed these cross-infection events in ~0.7% of dually infected cells (n = 22 events out of 3,153 dual-infected cells analyzed). After quantifying the fluorescence during each cross-infection event (Figure 4C), we identified a characteristic 3 h time window between the peak of donor phage induction (peak 1) and recipient phage infection (peak 2) (Figure 4D).

We confirmed that the cross-infection event happened only after recipient bacteria were engulfed by macrophages, and donor lysis had occurred. The bacteriophage lysis reporter only peaked in expression inside the recipient strain after full clearance of the donor bacterium, as shown in the lack of mCerulean signal at 6.7 h post-infection when the phage reporter peaks within the non-lysogenic cells (Figure 4C). Across all examples, the mCerulean signal level during peak 2 was close to zero (Figure 4E). At random, 22 control cells were chosen where macrophages were co-infected with both strains, but cross-infection did not occur. In these cells, during the last peak of phage induction, typically late activation of a lysogen, there was still more than 50% of mCerulean signal left on average (Figure 4E). As a further control, we screened a manually curated set of 614 macrophages that phagocytosed only the recipient bacterium during the dual infection (lower right quadrant in Figure S4J). All recipient-only-infected macrophages were negative for phage

(B) An example cell with successful cross-infection. The top row is a composite of the miRFP670 nuclear marker (blue), the mCerulean3 lysogen (light blue), the mClover recipient (green), and the mKate phage reporter signals (red). The white outline shows regions of the image with detectable phage reporter signal. Scale bar, 2 μm. (Bi) The lysogen (donor) strain and non-lysogen (recipient) strain co-infect the same macrophage. (Bii) The donor induces prophage. (Biii) Donors lyse. (Biv) More donors lyse while recipients replicate. (Bv) Phage infects and replicates in recipients. (Bvi) Donors are cleared, and phage replication continues in recipients. (Bvii) The recipients lyse from phage infection.

(C) The maximum mKate, mCerulean3, and mClover intensities measured over time for the bacterial masks associated with the cell in (B), normalized to highest maximal intensity. Black stars indicate time points shown in (B).

(D) For n = 22 single-cell examples with cross-infection across three experiments, the phage reporter was traced. Peak 1 denotes the time of the last phage induction by donor bacteria, and peak 2 denotes the time of the maximal phage replication in the recipient strain.

(E) For the 22 single cells exhibiting cross-infection, the residual mCerulean3 donor signal under the bacterial mask of the recipient strain was measured at the time of phage peak 2 (see Figure 4B, column vi: mCerulean intensity under mClover bacterial mask at maximal mKate signal). As a control, for 22 cells infected with both the donor and recipient strains that did not undergo cross-infection, where the mCerulean3 donor strain had more than one phage reporter peak, the mCerulean3 strain signal was measured across the whole cell at the time of phage peak 2.

See also Figure S4; Video S5.

reporter signal above the threshold throughout the entire time course—indicating that no infection of the recipient strain occurred prior to phagocytosis. These results demonstrate that functional phages are produced while bacteria are in an intracellular compartment—leading to propagation of secondary infection.

DISCUSSION

In this work, we demonstrate that a macrophage cell line triggers the induction of functional λ prophages from *E. coli* lysogens, using live-cell imaging and an approach to engineering whole lysogenic phage chromosomes. We identified that functional λ prophage induction leads to multiple mechanisms of bacterial clearance by the macrophage: bacterial cell death by phage lysis (Figures 2 and 3), and bacterial cell death by infecting phage produced by a neighboring induced bacterium (Figure 4). Our work emphasizes the need to study the mechanism of phage induction in physiologically relevant environments. For example, long-standing literature has postulated that the inducer of prophages during bacterial infection of mice is H_2O_2, a by-product of phagosomal enzymes and a known activator of the RecA-mediated SOS response (Figueroa-Bossi and Bossi, 1999). Our observations in live macrophage cells suggest the opposite—that DNA damage and RecA are not the main inducers of phage—as indicated by a higher induction frequency in the Δ*recA* mutant. That RecA is not the main trigger of induction inside phagosomes is consistent with the discrepancy between H_2O_2 concentrations used in *in vitro* studies versus estimated in the phagosome (>250 μM versus 1–4 μM, Goerlich et al., 1989; Slauch, 2011). Instead, we identified that native components of the murine phagosomal environment, such as mCramp1, can stimulate prophage induction through PhoP, suggesting that these interactions may occur in other cell types with cathelicidin-derived AMPs.

Our results demonstrate that the temperate, non-pathogenic bacteriophage λ may synergize with the innate immune system. Others have shown that *E. coli* lytic phages adhere to mucus to protect the gut epithelium and that *Clostridium difficile* phages kill the pathogen more effectively in combination with epithelial cells than in pure culture (Barr et al., 2013; Shan et al., 2018). Furthermore, computational modeling has demonstrated that immune-phage synergy is critical for the efficacy of bacteriophage therapy against *Pseudomonas aeruginosa* infection (Roach et al., 2017). In contrast, certain bacteriophages were shown to enhance the ability of *P. aeruginosa* to evade innate dendritic cells (Sweere et al., 2019). Thus, we anticipate that each phage-bacterium pairing has different interactions and consequences—and that these interactions also vary across various mammalian cell types, within the context of the entire host organism.

Similarly, our finding that the PhoP-mediated pathway is beneficial for prophage induction, rather than harmful (Alteri et al., 2011), may depend on the bacterial strain, or more particularly, its pathogenicity. Given that pathogenic *E. coli* and *L. monocytogenes* both express virulence genes from prophages without forming functional phage particles (demonstrated when bacteria are in a mouse or phagosome, respectively), perhaps pathogenic bacteria selectively induce prophage genes without allowing the full phage life cycle to progress (Balasubramanian et al., 2019; Rabinovich et al., 2012). One might expect the starvation-sensing and phage-inducing effects of PhoP to be decoupled in such strains. Further investigation of the specific signaling downstream of PhoP that connects to prophage induction in both pathogens and non-pathogens is needed.

High-throughput imaging allowed us to witness rare events, such as bacteriophage cross-infection inside living macrophages. Previous reports indirectly suggested the possibility of cross-infection, as RAW264.7 cells co-infected with a pathogen, *Mycobacterium tuberculosis*, and a non-pathogenic strain carrying an active phage infection, cleared more *M. tuberculosis* than when infected with *M. tuberculosis* alone (Broxmeyer et al., 2002); high-throughput fluorescence microscopy enabled us to demonstrate this phenomenon in real time. Furthermore, the low frequency of phage transfers inside the phagosome we observed may be underestimated, due to the re-infection defect of λ mKate and may also be due to physical containment of bacteria in separate phagosomes. A higher-resolution picture of phagosome biology will help elucidate the limitations of phage transfer inside macrophages.

We anticipate that bacteriophage transfer in the phagosome may alter macrophage function either during the course of an active bacterial infection or interaction with commensal bacteria. For example, the human colon contains more than 10^{13} bacterial cells (Sender et al., 2016), more than half of which are lysogenic (Kim and Bae, 2018) and have the potential to interact with greater than 10^7 intestinal macrophages ($\sim 10^5$ in mouse colon adjusted to volume of human colon; Denning et al., 2011). Phage particles produced in the phagosome have the potential to reach other compartments of the cell—the stability and likelihood of which may rely on proteases in the lysosome and cytosol (Volcy and Dewhurst, 2009). Endosomal phage particles have been demonstrated to stimulate TLR9 leading to anti-viral cytokine upregulation in dendritic cells (Gogokhia et al., 2019). Beyond immune stimulation, intracellular particles can enter the nucleus and function inside mammalian cells, as demonstrated by native phage RNA transcription (Sweere et al., 2019; Merril et al., 1971) and the finding of eukaryotic DNA sequences packaged in natural phage genomes (Bordenstein and Bordenstein, 2016). We predict within the context of bacterial-delivered phages that any of these events are likely to occur *in vivo* as we observed prophage induction in up to 20% of *E. coli*-infected macrophages. More mechanistic characterization of induction inside immune cells, together with the lysogenic phage engineering approach described here, will allow for a better understanding of the broader role phages play in the microbiome and in human health.

STAR★METHODS

Detailed methods are provided in the online version of this paper and include the following:

- KEY RESOURCES TABLE
- LEAD CONTACT AND MATERIALS AVAILABILITY

SUPPLEMENTAL INFORMATION

Supplemental Information can be found online at https://doi.org/10.1016/j.cels.2020.02.006.

ACKNOWLEDGMENTS

We gratefully acknowledge funding from the Allen Discovery Center grant to M.W.C. from the Paul G. Allen Frontiers Group. We further acknowledge the following support: Gabilan Stanford Graduate Fellowship (K.B.), Fannie and John Hertz Foundation Fellowship - Hertz-Draper Fellow (K.B.), Stanford EDGE-STEM Doctoral Fellowship (K.B.), and Nakajima Foundation Scholarship (T.K.). We would also like to thank members of the Covert lab, including M. DeFelice, for discussions and providing feedback on this work, along with D. Monack for helpful suggestions about the mCramp1 peptide and K.C. Huang and D. Endy for helpful comments. We would also like to thank the following people for contributing materials to this work: Nicolas Quach and David Van Valen for the *cI857* λ bacteriophage used in this paper, Keara Lane for the constitutive green fluorescent protein expression plasmid used in the recipient strain, the Onn Brandman Lab for the yeast BY4741 strain, the Rob Phillips lab for the LE392 strain, and Erin Schwartz for the pRS415 plasmid. Some of the computing for this project was performed on the Sherlock cluster. We would like to thank Stanford University and the Stanford Research Computing Center for providing computational resources and support that contributed to these research results. Additionally, we would like to thank the Stanford FACS facility for help with cell sorting.

AUTHOR CONTRIBUTIONS

Conceptualization, K.B., Y.T., and M.W.C.; Methodology, K.B., A.L.M., Y.T., and M.W.C.; Software, K.B. and T.K.; Investigation, K.B., A.I.M.B., and A.L.M.; Writing – Original Draft, K.B. and M.W.C.; Writing – Review & Editing, K.B., A.I.M.B., A.L.M., Y.T., T.K., and M.W.C.; Funding Acquisition, Y.T., T.K., and M.W.C; Supervision, M.W.C.

DECLARATION OF INTERESTS

The authors declare no competing interests.

Received: September 20, 2019
Revised: January 21, 2020
Accepted: February 18, 2020
Published: March 18, 2020

REFERENCES

Alteri, C.J., Lindner, J.R., Reiss, D.J., Smith, S.N., and Mobley, H.L.T. (2011). The broadly conserved regulator PhoP links pathogen virulence and membrane potential in Escherichia coli. Mol. Microbiol. *82*, 145–163.

Ando, H., Lemire, S., Pires, D.P., and Lu, T.K. (2015). Engineering modular viral scaffolds for targeted bacterial population editing. Cell Syst. *1*, 187–196.

Baba, T., Ara, T., Hasegawa, M., Takai, Y., Okumura, Y., Baba, M., Datsenko, K.A., Tomita, M., Wanner, B.L., and Mori, H. (2006). Construction of Escherichia coli K-12 in-frame, single-gene knockout mutants: the Keio collection. Mol. Syst. Biol. *2*, 2006.0008.

Balasubramanian, S., Osburne, M.S., BrinJones, H., Tai, A.K., and Leong, J.M. (2019). Prophage induction, but not production of phage particles, is required for lethal disease in a microbiome-replete murine model of enterohemorrhagic *E. coli* infection. PLoS Pathog. *15*.

Barr, J.J. (2017). A bacteriophages journey through the human body. Immunol. Rev. *279*, 106–122.

Barr, J.J., Auro, R., Furlan, M., Whiteson, K.L., Erb, M.L., Pogliano, J., Stotland, A., Wolkowicz, R., Cutting, A.S., Doran, K.S., et al. (2013). Bacteriophage adhering to mucus provide a non-host-derived immunity. Proc. Natl. Acad. Sci. USA *110*, 10771–10776.

Bassøe, C.F., and Bjerknes, R. (1985). Phagocytosis by human leukocytes, phagosomal pH and degradation of seven species of bacteria measured by flow cytometry. J. Med. Microbiol. *19*, 115–125.

Bordenstein, S.R., and Bordenstein, S.R. (2016). Eukaryotic association module in phage WO genomes from Wolbachia. Nat. Commun. *7*, 13155.

Broxmeyer, L., Sosnowska, D., Miltner, E., Chacón, O., Wagner, D., McGarvey, J., Barletta, R.G., and Bermudez, L.E. (2002). Killing of *Mycobacterium avium* and *Mycobacterium tuberculosis* by a mycobacteriophage delivered by a nonvirulent Mycobacterium: a model for phage therapy of intracellular bacterial pathogens. J. Infect. Dis. *186*, 1155–1160.

Chapon, C. (1982). Role of the catabolite activator protein in the maltose regulon of Escherichia coli. J. Bacteriol. *150*, 722–729.

Cranfill, P.J., Sell, B.R., Baird, M.A., Allen, J.R., Lavagnino, Z., de Gruiter, H.M., Kremers, G.J., Davidson, M.W., Ustione, A., and Piston, D.W. (2016). Quantitative assessment of fluorescent proteins. Nat. Methods *13*, 557–562.

De Paepe, M., Tournier, L., Moncaut, E., Son, O., Langella, P., and Petit, M.A. (2016). Carriage of λ latent virus is costly for its bacterial host due to frequent reactivation in monoxenic Mouse Intestine. PLoS Genet. *12*, e1005861.

Denning, T.L., Norris, B.A., Medina-Contreras, O., Manicassamy, S., Geem, D., Madan, R., Karp, C.L., and Pulendran, B. (2011). Functional specializations of intestinal dendritic cell and macrophage subsets that control Th17 and regulatory T cell responses are dependent on the T cell/APC ratio, source of mouse strain, and regional localization. J. Immunol. *187*, 733–747.

Diard, M., Bakkeren, E., Cornuault, J.K., Moor, K., Hausmann, A., Sellin, M.E., Loverdo, C., Aertsen, A., Ackermann, M., De Paepe, M., et al. (2017). Inflammation boosts bacteriophage transfer between Salmonella spp. Science *355*, 1211–1215.

Farris, C., Sanowar, S., Bader, M.W., Pfuetzner, R., and Miller, S.I. (2010). Antimicrobial peptides activate the Rcs regulon through the outer membrane lipoprotein RcsF. J. Bacteriol. *192*, 4894–4903.

Figueroa-Bossi, N., and Bossi, L. (1999). Inducible prophages contribute to Salmonella virulence in mice. Mol. Microbiol. *33*, 167–176.

Flannagan, R.S., Cosío, G., and Grinstein, S. (2009). Antimicrobial mechanisms of phagocytes and bacterial evasion strategies. Nat. Rev. Microbiol. *7*, 355–366.

Gallo, R.L., Kim, K.J., Bernfield, M., Kozak, C.A., Zanetti, M., Merluzzi, L., and Gennaro, R. (1997). Identification of CRAMP, a cathelin-related antimicrobial peptide expressed in the embryonic and adult mouse. J. Biol. Chem. *272*, 13088–13093.

Garcia-del Portillo, F., Foster, J.W., Maguire, M.E., and Finlay, B.B. (1992). Characterization of the micro-environment of *Salmonella typhimurium*-containing vacuoles within MDCK epithelial cells. Mol. Microbiol. *6*, 3289–3297.

Goerlich, O., Quillardet, P., and Hofnung, M. (1989). Induction of the SOS response by hydrogen peroxide in various Escherichia coli mutants with altered protection against oxidative DNA damage. J. Bacteriol. *171*, 6141–6147.

Gogokhia, L., Buhrke, K., Bell, R., Hoffman, B., Brown, D.G., Hanke-Gogokhia, C., Ajami, N.J., Wong, M.C., Ghazaryan, A., Valentine, J.F., et al. (2019). Expansion of bacteriophages is linked to aggravated intestinal inflammation and colitis. Cell Host Microbe *25*, 285–299.e8.

Gut, H., Pennacchietti, E., John, R.A., Bossa, F., Capitani, G., De Biase, D., and Grütter, M.G. (2006). Escherichia coli acid resistance: pH-sensing, activation by chloride and autoinhibition in GadB. EMBO J. *25*, 2643–2651.

Hodyra-Stefaniak, K., Miernikiewicz, P., Drapała, J., Drab, M., Jończyk-Matysiak, E., Lecion, D., Kaźmierczak, Z., Beta, W., Majewska, J., Harhala, M., et al. (2015). Mammalian Host-versus-phage immune response determines phage fate in vivo. Sci. Rep. *5*, 14802.

Imamovic, L., and Muniesa, M. (2012). Characterizing RecA-independent induction of Shiga toxin2-encoding phages by EDTA treatment. PLoS One *7*, e32393.

Keen, E.C., and Dantas, G. (2018). Close encounters of three kinds: bacteriophages, commensal bacteria, and host immunity. Trends Microbiol. *26*, 943–954.

Kim, M.S., and Bae, J.W. (2018). Lysogeny is prevalent and widely distributed in the murine gut microbiota. ISME J. *12*, 1127–1141.

Kudo, T., Jeknić, S., Macklin, D.N., Akhter, S., Hughey, J.J., Regot, S., and Covert, M.W. (2018). Live-cell measurements of kinase activity in single cells using translocation reporters. Nat. Protoc. *13*, 155–169.

Lane, K., Andres-Terre, M., Kudo, T., Monack, D.M., and Covert, M.W. (2019). Escalating threat levels of bacterial infection can be discriminated by distinct MAPK and NF-κB signaling dynamics in single host cells. Cell Syst. *8*, 183–196.e4.

Lieb, M. (1966). Studies of heat-inducible lambda bacteriophage: I. order of genetic sites and properties of mutant prophages. J. Mol. Biol. *16*, 149–163.

Liu, X., Jiang, H., Gu, Z., and Roberts, J.W. (2013). High-resolution view of bacteriophage lambda gene expression by ribosome profiling. Proc. Natl. Acad. Sci. USA *110*, 11928–11933.

Madera, C., García, P., Rodríguez, A., Suárez, J.E., and Martínez, B. (2009). Prophage induction in Lactococcus lactis by the bacteriocin lactococcin 972. Int. J. Food Microbiol. *129*, 99–102.

Majdalani, N., and Gottesman, S. (2005). THE RCS phosphorelay: a complex signal transduction system. Annu. Rev. Microbiol. *59*, 379–405.

Manrique, P., Bolduc, B., Walk, S.T., van der Oost, J., de Vos, W.M., and Young, M.J. (2016). Healthy human gut phageome. Proc. Natl. Acad. Sci. USA *113*, 10400–10405.

Matsushiro, A., Sato, K., Miyamoto, H., Yamamura, T., and Honda, T. (1999). Induction of prophages of enterohemorrhagic Escherichia coli O157:H7 with norfloxacin. J. Bacteriol. *181*, 2257–2260.

Maynard, N.D., Birch, E.W., Saghvi, J.C., Chen, L., Gutschow, M.V., and Covert, M.W. (2010). A forward-genetic screen and dynamic analysis of lambda phage host-dependencies reveals an extensive interaction network and a new anti-viral strategy. PLoS Genet *6*, e1001017.

Merril, C.R., Geier, M.R., and Petricciani, J.C. (1971). Bacterial virus gene expression in human cells. Nature *233*, 398–400.

Mirzaei, M.K., and Maurice, C.F. (2017). Ménage à trois in the human gut: interactions between host, bacteria and phages. Nat. Rev. Microbiol. *15*, 397–408.

Monsieurs, P., De Keersmaecker, S., Navarre, W.W., Bader, M.W., De Smet, F., McClelland, M., Fang, F.C., De Moor, B., Vanderleyden, J., and Marchal, K. (2005). Comparison of the PhoPQ regulon in Escherichia coli and Salmonella typhimurium. J. Mol. Evol. *60*, 462–474.

Nanda, A.M., Thormann, K., and Frunzke, J. (2015). Impact of spontaneous prophage induction on the fitness of bacterial populations and host-microbe interactions. J. Bacteriol. *197*, 410–419.

Nikaido, H. (2003). Molecular basis of bacterial outer membrane permeability revisited. Microbiol. Mol. Biol. Rev. *67*, 593–656.

Oh, J.H., Alexander, L.M., Pan, M., Schueler, K.L., Keller, M.P., Attie, A.D., Walter, J., and Van Pijkeren, J.P. (2019). Dietary fructose and microbiota-derived short-chain fatty acids promote bacteriophage production in the gut symbiont *Lactobacillus reuteri*. Cell Host Microbe *25*, 273–284.e6.

Pires, D.P., Cleto, S., Sillankorva, S., Azeredo, J., and Lu, T.K. (2016). Genetically engineered phages: a review of advances over the last decade. Microbiol. Mol. Biol. Rev. *80*, 523–543.

Rabinovich, L., Sigal, N., Borovok, I., Nir-Paz, R., and Herskovits, A.A. (2012). Prophage excision activates Listeria competence genes that promote phagosomal escape and virulence. Cell *150*, 792–802.

Roach, D.R., Leung, C.Y., Henry, M., Morello, E., Singh, D., Di Santo, J.P., Weitz, J.S., and Debarbieux, L. (2017). Synergy between the host immune system and bacteriophage is essential for successful phage therapy against an acute respiratory pathogen. Cell Host Microbe *22*, 38–47.e4.

Ronneberger, O., Fischer, P., and Brox, T. (2015). U-net: convolutional networks for biomedical image segmentation. In Medical Image Computing and Computer Assisted Intervention MICCAI 2015, *vol 9351*, N. Navab, J. Hornegger, W. Wells, and A. Frangi, eds. (Springer), pp. 234–241.

Rozanov, D.V., D'Ari, R., and Sineoky, S.P. (1998). RecA-independent pathways of lambdoid prophage induction in Escherichia coli. J. Bacteriol. *180*, 6306–6315.

Schindelin, J., Arganda-Carreras, I., Frise, E., Kaynig, V., Longair, M., Pietzsch, T., Preibisch, S., Rueden, C., Saalfeld, S., Schmid, B., et al. (2012). Fiji: an open-source platform for biological-image analysis. Nat. Methods *9*, 676–682.

Sender, R., Fuchs, S., and Milo, R. (2016). Revised estimates for the number of human and bacteria cells in the body. PLoS Biol. *14*, e1002533.

Shan, J., Ramachandran, A., Thanki, A.M., Vukusic, F.B.I., Barylski, J., and Clokie, M.R.J. (2018). Bacteriophages are more virulent to bacteria with human cells than they are in bacterial culture; insights from HT-29 cells. Sci. Rep. *8*, 5091.

Shcherbakova, D.M., Baloban, M., Emelyanov, A.V., Brenowitz, M., Guo, P., and Verkhusha, V.V. (2016). Bright monomeric near-infrared fluorescent proteins as tags and biosensors for multiscale imaging. Nat. Commun. *7*, 12405.

Skinner, S.O., Sepúlveda, L.A., Xu, H., and Golding, I. (2013). Measuring mRNA copy number in individual Escherichia coli cells using single-molecule fluorescent in situ hybridization. Nat. Protoc. *8*, 1100–1113.

Skurnik, M., and Strauch, E. (2006). Phage therapy: facts and fiction. Int. J. Med. Microbiol. *296*, 5–14.

Slauch, J.M. (2011). How does the oxidative burst of macrophages kill bacteria? Still an open question. Mol. Microbiol. *80*, 580–583.

Sweere, J.M., Van Belleghem, J.D., Ishak, H., Bach, M.S., Popescu, M., Sunkari, V., Kaber, G., Manasherob, R., Suh, G.A., Cao, X., et al. (2019). Bacteriophage trigger antiviral immunity and prevent clearance of bacterial infection. Science *363*, https://doi.org/10.1126/science.aat9691.

Trinh, J.T., Székely, T., Shao, Q., Balázsi, G., and Zeng, L. (2017). Cell fate decisions emerge as phages cooperate or compete inside their host. Nat. Commun. *8*, 14341.

Van Belleghem, J.D., Dąbrowska, K., Vaneechoutte, M., Barr, J.J., and Bollyky, P.L. (2018). Interactions between bacteriophage, bacteria, and the mammalian immune system. Viruses *11*, https://doi.org/10.3390/v11010010.

Van Valen, D.A., Kudo, T., Lane, K.M., Macklin, D.N., Quach, N.T., DeFelice, M.M., Maayan, I., Tanouchi, Y., Ashley, E.A., and Covert, M.W. (2016). Deep learning automates the quantitative analysis of individual cells in live-cell imaging experiments. PLoS Comput. Biol. *12*, e1005177.

Volcy, K., and Dewhurst, S. (2009). Proteasome inhibitors enhance bacteriophage lambda (lambda) mediated gene transfer in mammalian cells. Virology *384*, 77–87.

Yu, X.J., Liu, M., and Holden, D.W. (2004). SsaM and SpiC interact and regulate secretion of salmonella pathogenicity island 2 type III secretion system effectors and translocators. Mol. Microbiol. *54*, 604–619.

STAR★METHODS

KEY RESOURCES TABLE

REAGENT or RESOURCE	SOURCE	IDENTIFIER
Bacterial and Virus Strains		
Escherichia coli strain MG1655	Coli Genetic Stock Center	CGSC#7740
Escherichia coli strain BW25113	Baba et al., 2006	N/A
Escherichia coli strain LE392	Gift from the Rob Phillips Lab (Caltech)	N/A
Escherichia coli strain MG1655/PE003	This paper	N/A
Escherichia coli strain BW25113/PE003	This paper	N/A
Escherichia coli strain LE392/PE003	This paper	N/A
Escherichia coli strain LE392/KL248	This paper	N/A
Escherichia coli strain MG1655 attB::[λ-mKate *cI* (WT)]/ PE003	This paper	N/A
Escherichia coli strain MG1655 attB::[λ-mKate-parS *cI* (WT)]/ PE003	This paper	N/A
Escherichia coli strain BW25113 attB::[λ-mKate *cI* (WT)]/ PE003	This paper	N/A
Escherichia coli strain LE392 attB::[λ-mKate (*cI857*)]/PE003	This paper	N/A
Escherichia coli strain BW25113 Δ*recA*::*kan*	Baba et al., 2006	N/A
Escherichia coli strain BW25113 Δ*gadB*::*kan*	Baba et al., 2006	N/A
Escherichia coli strain BW25113 Δ*phoP*::*kan*	Baba et al., 2006	N/A
Escherichia coli strain BW25113 Δ*rcsA*::*kan*	Baba et al., 2006	N/A
Escherichia coli strain BW25113 Δ*recA*::FRT	This paper	N/A
Escherichia coli strain BW25113 Δ*gadB*::FRT	This paper	N/A
Escherichia coli strain BW25113 Δ*phoP*::FRT	This paper	N/A
Escherichia coli strain BW25113 Δ*rcsA*::FRT	This paper	N/A
Escherichia coli strain BW25113 Δ*recA*::FRT/PE003	This paper	N/A
Escherichia coli strain BW25113 Δ*gadB*::FRT/PE003	This paper	N/A
Escherichia coli strain BW25113 Δ*phoP*::FRT/PE003	This paper	N/A
Escherichia coli strain BW25113 Δ*rcsA*::FRT/PE003	This paper	N/A
Escherichia coli strain BW25113 Δ*recA*::FRT attB::[λ-mKate *cI* (WT)/PE003	This paper	N/A
Escherichia coli strain BW25113 Δ*gadB*::FRT attB::[λ-mKate *cI* (WT)/PE003	This paper	N/A
Escherichia coli strain BW25113 Δ*phoP*::FRT attB::[λ-mKate *cI* (WT)/PE003	This paper	N/A
Escherichia coli strain BW25113 Δ*rcsA*::FRT attB::[λ-mKate *cI* (WT)/PE003	This paper	N/A
Escherichia coli strain MG1655/pUC19	This paper	N/A
Bacteriophage λ	ATCC	Cat#23724-B2
Bacteriophage λ Δ*bor*::*kan cI*857	Gift from the Lanying Zeng Lab (TAMU)	N/A
Bacteriophage λ-mKate: *cI* (WT) Δ*bor::kan*, RBS-mKate2, Δ[*ea31,ea59*]::PGK-mClover-bgh terminator	This paper	N/A
Bacteriophage λ-KB001: *cI* (WT) Δ*bor::kan*, Δ[*ea31,ea59*]::PGK-mClover-bgh terminator	This paper	N/A

(*Continued on next page*)

Continued

REAGENT or RESOURCE	SOURCE	IDENTIFIER
Bacteriophage λ-mKate-parS: *cI* (WT) Δ*bor::kan*, RBS-mKate2-parS	This paper	N/A
Bacteriophage λ-mKate *cI857*: *Sam7*, Δ*bor::kan*, RBS-mKate2, Δ[*ea31,ea59*]::PGK-mClover-bgh terminator, pRM-mNeonGreen	Gift from Nicolas Quach (Stanford)	N/A
Chemicals, Peptides, and Recombinant Proteins		
FluoroBrite™ DMEM	Life Technologies	Cat#A1896702
Fibronectin	Sigma-Aldrich	Cat#F0895-5MG
Hygromycin B	Thermo Fisher Scientific	Cat#10687010
Gentamicin	Thermo Fisher Scientific	Cat#15710064
Norfloxacin	Sigma-Aldrich	Cat#N9890-5G
Mitomycin C from *Streptomyces caespitosus*	Sigma-Aldrich	Cat#M4287-2MG
gelatin from porcine skin, Type A	Sigma-Aldrich	Cat#G1890-100G; Cas#9000-70-8
mCramp, mouse	Anaspec	Cat#AS-61305
Critical Commercial Assays		
DNeasy Blood and Tissue Kit	Qiagen	Cat#69504
YeaStar™ Genomic DNA Kit	Zymo Research	Cat# D2002
Deposited Data		
Raw and analyzed data and analysis scripts	This paper	https://doi.org/10.17632/f5jpffyhmg.1
Experimental Models: Cell Lines		
Mouse: RAW264.7 cells (male)	ATCC	Cat#TIB-71; RRID:CVCL_0493
Mouse: RAW264.7 cells (male), pGK-HygroR,pGK-H2B-miRFP670	This paper	N/A
Human: 293FT (female)	Thermo Fisher Scientific	Cat#R700-07
Experimental Models: Organisms/Strains		
Saccharomyces cerevisiae strain BY4741, *MATa his3Δ1 leu2Δ met15Δ ura3Δ*	Gift from the Onn Brandman Lab (Stanford)	N/A
Oligonucleotides		
Primers for recombinant phage construction and validation and Keio strain validation, see Table S1B	This paper	N/A
Recombinant DNA		
Plasmid PE003: SC101 (CmR) - J23119-B0030-mCerulean3	This paper	N/A
Plasmid KL248: SC101 (CmR) - J23119-B0034-mClover (mClover plasmid used with recipient strain in Figure 4)	Gift from Keara Lane (Northwestern University)	N/A
Plasmid PE022: (AmpR) -pLenti-pGK-HygroR-pGK-H2B-miRFP670 (lentiviral)	This paper	N/A
Plasmid pmiRFP670-N1	Addgene	Addgene#79987
Plasmid pCP20	*E. coli* Genetic Stock Center	Cat#64621
Plasmid pRS415 (yeast centromere plasmid for expression of LEU2, with bacterial origin of replication), (AmpR)- LEU2, CEN/ARS (*S. cerevisiae* centromere CEN6 fused to replicating sequence)	Gift from Erin Schwartz (Stanford)	N/A
Plasmid pUC19	Thermo Fisher Scientific	Cat#SD0061
Plasmid PE005: p15A: pL-mKate-LVA	This paper	N/A
Software and Algorithms		
CellTK	Kudo et al., 2018	https://github.com/CovertLab/CellTK
Covertrace	Kudo et al., 2018	https://github.com/CovertLab/covertrace
CellUNet	Created by Takamasa Kudo, This paper	https://github.com/CovertLab/cellunet

(*Continued on next page*)

Continued

REAGENT or RESOURCE	SOURCE	IDENTIFIER
Python, version 2.7		https://www.python.org
Seaborn		https://seaborn.pydata.org/index.html
FIJI	Schindelin et al., 2012	https://fiji.sc/
Other		
Nunc™ Microwell™ 96-Well Optical-Bottom Plates with Coverglass Base	Thermo Fisher Scientific	Cat#164588
AeraSeal™ film	Sigma-Aldrich	Cat#A9224
Falcon™ Polystyrene Microplates	Fisher Scientific	Cat#08-772-1B
Fisherbrand™ Electroporation Cuvettes Plus	Fisher Scientific	Cat# FB101
Thermo Scientific™ Nunc™ Lab-Tek™ Chambered Coverglass	Fisher Scientific	Cat#12-565-472
CELLSTAR® Tissue Culture Plates, Greiner Bio-One	VWR	Cat#655161

LEAD CONTACT AND MATERIALS AVAILABILITY

Further information and requests for resources and reagents should be directed to and will be fulfilled by the Lead Contact, Markus Covert (mcovert@stanford.edu). All plasmids generated in this study will be available on Addgene (https://www.addgene.org/Markus_Covert/) and all other unique/stable reagents will be available by request from the Lead Contact with a completed Materials Transfer Agreement.

EXPERIMENTAL MODEL AND SUBJECT DETAILS

Mammalian Cell Lines and Cell Culture

The RAW264.7-H2B-miRFP (male) cells were cultured in DMEM (Thermo Fisher Scientific, 11965-118) with 10% FBS (Omega Scientific), 2 mM L-Glutamine (Life Technologies), and 1X Penicillin/Streptomycin (Life Technologies) at 37°C, 5% CO_2. These cells were derived from RAW264.7 (RRID:CVCL_0493) cells from ATCC.

Lentivirus was generated using 293FT (female) cells from Thermo Fisher Scientific. These were maintained in DMEM supplemented with 10% FBS (Omega Scientific), 2 mM L-Glutamine (Life Technologies), and 1X Penicillin/Streptomycin (Life Technologies), 1% MEM Non-Essential Amino Acids (Sigma) and 1 mM Sodium Pyruvate (Sigma) at 37°C, 5% CO_2.

The RAW264.7 cells were infected with lentivirus expressing H2B-miRFP670, along with a hygromycin resistance marker, grown under 250 μg/mL hygromycin selection and further sorted. The lentivirus generated from plasmid PE022 was constructed based off of Addgene plasmid, pmiRFP670-N1. This was a gift from Vladislav Verkhusha (Addgene plasmid # 79987) (Shcherbakova et al., 2016). No cell lines were authenticated.

For live-cell imaging, cells were maintained in imaging media (IM) (Fluorobrite + 10 mM HEPES pH=7.0 (Sigma) + 1% FBS + 2 mM L-glutamine).

Bacterial Cell Lines and Culture

Unless indicated otherwise, all *E. coli* cell lines (BW25113, MG1655 and LE392) were grown with aeration in Miller's LB Broth (RPI) at 37°C. M9 minimal medium (1x M9 salts (BD), 2 mM $MgSO_4$ (Sigma Aldrich), 100 μM $CaCl_2$ (EMD)) supplemented with 22 mM glucose (Sigma) was used to create the agar pads to minimize auto-fluorescence. For media comparison experiments in Figure S4, derivatives of MgM-MES (Yu et al., 2004) (pH = 5.8, Mg^{2+} = 8 mM) and M–MES (pH = 7.0, Mg^{2+} = 40 μM) were also used. The base M-MES medium contained: 170 mM MES (2-[N-morpholino] ethane-sulphonic acid at pH = 5.0, Sigma Aldrich), 5 mM KCl (Sigma), 7.5 mM $(NH_4)_2SO_4$ (Sigma), 0.5 mM K_2SO_4 (Sigma Aldrich), 1 mM KH_2PO_4 (Fisher RPI), 2 mM Glucose (Sigma, G8270), 0.1% casamino acids (Thermo Fisher Scientific). Mg^{2+} was supplemented as $MgCl_2$ (Fisher). MgM-MES and M-MES media compositions were motivated by conditions estimated inside cells. The pH is estimated to be 5.3 in human monocyte phagolysosomes, and Mg^{2+} is estimated to be between 10-50 μM in bacterial vacuoles in epithelial cells (Bassøe and Bjerknes, 1985; Garcia-del Portillo et al., 1992).

For the mCramp1 peptide stimulation experiments, E-LB (LB + 11-mM glucose + 10 mM Mg^{2+}) was used for exponential phase growth. We chose to test the peptide in E-LB to isolate the influence of mCramp1 on outer membrane stability without any additional limitations of LB medium. Mg^{2+} stabilizes lipopolysaccharides (LPS) in the cell wall of bacteria at millimolar concentrations, so we supplemented the E-LB medium with high Mg^{2+} (Reviewed in Nikaido, 2003). We also supplemented the medium with glucose, which represses the expression of LamB, the λ receptor, such that phages cannot re-infect the same bacterial population, leading to reporter activation not involved with prophage induction (Chapon, 1982). For the growth curves with phage infection, Nutrient Broth (NB) media was used (Sigma).

Unless indicated otherwise, antibiotics were applied at: 100 μg/mL carbenicillin (Fisher), 50 μg/mL kanamycin (Fisher), 20 μg/mL chloramphenicol (Sigma-Aldrich), 10 μg/mL gentamicin (Thermo Fisher Scientific). Inducers were applied at the following concentrations:

norfloxacin (50 ng/mL, Sigma-Aldrich), mitomycin C (1 μg/mL, Sigma-Aldrich), mCramp1 (2 μM, Anaspec). For comparison, 1 μM is the minimum inhibitory concentration of mCramp1 in *E. coli* (Gallo et al., 1997). Furthermore, mCramp1 was synthesized fresh for each experiment due to instability of the peptide.

Bacteriophage Stocks and Propagation Culture

All bacteriophage λ stocks were stored long-term in the dark, at 4°C in SM media (100 mM NaCl (Fisher Scientific), 8 mM $MgSO_4$*$7H_20$ (Sigma-Aldrich), 50 mM Tris pH=7.5 (Life Technologies)) + 0.01% w/v gelatin from porcine skin, Type A (Sigma).

For plaque assays, *E. coli* were grown in TB medium: 10 g/L Bacto tryptone (Fisher Scientific), 5 g/L NaCl (Fisher Scientific). Propagation plates for phage lysis were created as follows: 1.2% Bacto Agar (Thermo Fisher Scientific, DF0140), 0.3% Glucose, 2 mM $MgSO_4$ (Sigma Aldrich), 0.075 mM $CaCl_2$ (EMD), 0.004 mM $FeCl_3$ (Sigma Aldrich), 0.01 mg/L Thiamine Hydrochloride (Sigma Aldrich).

Yeast Stocks and Culture

S. cerevisiae BY4741 yeast were maintained in YPD broth (Fisher (RPI)) or in SD-LEU medium (Minimal SD Base (Clontech) + (-His/-Leu/-Ura DO Supplement, Clontech) + 20 μg/mL L-Histidine (Sigma) + 20 μg/mL Uracil (Sigma)) after transformation at 30°C, 5% CO_2.

METHOD DETAILS

Generation of Recombinant Bacteriophages

The λ mKate phage was designed as described in (Figures 1A, 1B, and S1A; Table S1A) and assembled as seven fragments along with a Yeast Artificial Chromosome (YAC). The first design choice was which orientation of the genome to engineer: the packaged-in-particles form or the lysogenic, integrated-into-the-genome form. Since the entire phage genome is inserted into a YAC, we were unsure whether the particle form genome would excise from the YAC and package properly. Thus, we chose the genomic DNA orientation (Figure 1Ai) such that the phage can excise from the YAC and produce particles, just as it would from a bacterial chromosome (See Figure 1Aiv). All engineered phages also contained a Δ*bor::kan*, allowing for selection of kanamycin resistant lysogens after engineering (Figure 1Avii), since the YAC-phage construct lacks a bacterial origin of replication and cannot replicate in *E. coli*, validating the lytic and lysogenic functionality of the phage in one step.

All fragments were amplified by PCR using Phusion High-Fidelity DNA Polymerase (NEB) using the primer sets indicated in Table S1B. Fragment 5 also contained a mammalian cassette PGK promoter-mClover-2A-puroR-bghTerm in place of *ea31* and *ea59* that we had intended to use for downstream selection of mammalian cells with phage DNA. We validated that these lysogens do not express the mClover while on the agar pad or once inside the phagosome. The genomic DNA used as template for fragments was purified from BW25113 *E. coli* lysogenized for various λ variants including the WT and λ-Δ*bor::kan* (a gift from the lab of Lanying Zeng) using DNeasy Blood and Tissue kit (Qiagen). The YAC fragment was treated with DpnI (NEB) overnight to reduce background. All PCRs were purified with QIAquick PCR purification kit (Qiagen) prior to transformation and eluted in 15 μL H_2O to concentrate as highly as possible.

Next, the inserts were transformed into yeast. *S. cerevisiae* BY4741 was grown in 3 mL YPD at 30°C for 16 hours. Overnight cultures were diluted 1:10 into 30 mL of YPD and incubated at 30°C for 4 hours. Cells were centrifuged at 1000g, washed with 25 mL water and then with 1 mL of 100 mM lithium acetate (LiAc) (Sigma-Aldrich) and suspended in 240 μL of 100 mM LiAc. After resuspension in LiAc, competent cells were promptly used for transformation and not stored. All PCR products (as close as possible to 1 μg per fragment and 300 ng of YAC) were mixed in a tube up to 50 μL total, including added H_2O. The products were mixed with a transformation mixture (50 μL yeast competent cell, 240 μL 50% PEG3350 (Sigma-Aldrich), 36 μL 1 M LiAc, 25 μL 2 mg/mL salmon sperm DNA, which was boiled for 5 minutes (Invitrogen)). The mixture was vortexed well and then incubated at 30°C for 30 minutes in a rotating nutator, then at 42°C for 45 minutes, centrifuged at 8000g for 30 s, and suspended in 200 μL water. Transformants were selected on SD-LEU plates at 30°C for 3-5 days.

Transformants were screened for proper assembly (See Figures S1A and S1B). Yeast colonies were picked (usually 8 colonies) and resuspended in 30 μL of H_2O. 20 μL of colony suspensions (the rest saved for liquid growth) were mixed with 100 μL of 20 mM NaOH (Sigma) and were heated at 95°C for 10 minutes, vortexed and centrifuged at 8000g for 1 minute. 1 μL of lysate was used as template in a colony PCR reaction with each of the junction check primers as referenced in Table S1B using GoTaq Green Mastermix (Promega). For colonies that correctly contained all 7 junctions, 10 μL of suspension was inoculated in 20 mL of SD-LEU liquid medium and cultures were grown at 30°C for 3-5 days (until OD600 ~1.0 was reached). Yeast genomic DNA was extracted from a volume of cells containing OD600=10 equivalent from the liquid cultures using the YeaStar™ Genomic DNA Kit (Zymo Research) using Protocol I. PCR reactions for all junctions were performed once more with the 7 junction primer sets from Table S1B as in the initial screening to make sure that unwanted recombination did not occur during growth.

To isolate functional, recombinant phage particles, we took the approach to first generate and select lysogens. The extracted, validated yeast gDNA (2.5 μL) was electroporated into 25 μL of *E. coli* MegaX DH10B T1R Electrocomp Cells (Thermo Fisher Scientific) in a 1-mm gap electroporation cuvette (Fisher) at 2000 V, 25 μF, and 200 Ω using a Gene Pulser Xcell Microbial System (Bio-Rad). Cells

were mixed with 1 mL of Recovery Medium (Thermo Fisher Scientific) and recovered at 37°C for 3 hours and plated onto LB agar plates supplemented with kanamycin, to select for the kanamycin resistance in the phage, and grown for 16 hours at 37°C. The formation of kanamycin resistant lysogens suggests that the phage was able to excise from the YAC-phage construct, form particles and infect and lysogenize untransformed *E. coli*. Several colonies were picked per lysogen, suspended in H_2O and used as template in a colony PCR reaction with primers across the attR site (Table S1B) to validate that the attR site formed as a result of phage integration. A PCR reaction using the insert 6 primers was also performed across the mKate cassette, purified and sequenced to confirm there was no cross-contamination with WT λ to form the lysogens.

Recombinant λ mKate phage particles produced by the DH10B lysogens were isolated by detecting spontaneous induction when mixed with a susceptible indicator strain. Specifically, a plaque assay was performed with a mixture of the lysogen strain and plating cells, a phage-susceptible MG1655/pUC19 strain (for carbenicillin (Carb) resistance). Plating cells grown for 16 hours in LB at 37°C were diluted 100-fold into 20 mL TB + 0.2% maltose (EMD Chemicals) and cultured at 37°C until OD600=0.4. The cells were incubated on ice for 15 minutes, centrifuged at 3000g for 10 minutes at 4°C and resuspended in cold TB + 10 mM MgSO4 (Sigma Aldrich) to final OD600=2.0. The lysogens were grown for 16 hours in 3 mL LB + kanamycin and diluted 1:100 in E-LB and grown at 37°C until mid-exponential phase. The glucose should repress the LamB receptor for phage and prevent re-uptake of spontaneously produced particles, and Mg^{2+} functions to stabilize the phage particles produced (Chapon, 1982). 100 μL of plating cells and 100 μL of lysogen culture were mixed along with 3 mL of TB soft (0.7%) agar and plated onto TB Carb plates. The Carb allows a lawn of only the plating cells to grow, and any spontaneously produced particles should propagate as plaques. Several 'cloudy' plaques were picked and stored in 100 μL of SM+gelatin buffer. Once more, the phage was validated for presence of the mKate by PCR.

Next, phage particles were propagated by plate lysis to increase titer for lysogen creation. Briefly, MG1655/pUC19, the propagation host, from overnight culture in LB was diluted 100-fold into 20 mL TB and cultured until OD=0.4 at 37°C. The resuspended plaques were mixed with 1 mL of propagation host, incubated at 4°C for 15 minutes, and 350 μL of mixture was mixed with 3 mL of soft TB (0.7%) agar and plated onto propagation plates. Plates were incubated at 37°C without inversion until plaques covered the whole plate, typically < 5 hours. Phages were concentrated and harvested by elution method. Briefly, 5 mL of SM buffer was added to each plate and incubated for 2 hours on a shaking platform. The 5 mL of buffer was re-collected from the plate, and then, 1 mL of fresh SM was added back to the plate for 15 minutes at 4°C. The second SM harvest was combined with the first, mixed with 100 μL of Chloroform (Sigma Aldrich) and incubated at 24°C for 10 minutes. Lysates were centrifuged at 4000g at 4°C for 10 minutes. Titers were $\sim 10^{11}$ pfu/mL as determined by plaque assay with susceptible MG1655 host in serial dilutions onto TB soft agar.

The phage lysate was used to create lysogens with all relevant strains (MG1655, BW25113 and Keio derivatives and LE392). For the λ mKate (*cI857*), the genetic background had a Sam7 mutation, so we propagated this strain in an amber suppressor *E. coli* host – LE392. Parent strains were grown overnight in LB supplemented with the appropriate antibiotic and diluted 100-fold into fresh TB supplemented with 0.2% maltose and grown until early stationary phase, roughly 5 hours. The cells were centrifuged at 8000g for 1 minute at 24°C and were resuspended in 1 mL of 10 mM $MgSO_4$ to starve them and were then incubated for 1 hour at 30°C. 50 μL of cells were mixed with 50-μL phage at Multiplicity of Infection (MOI) 0.01 and incubated at 4°C for 30 minutes. The mixture of cells and phage was mixed with 900 μL of pre-warmed LB + 10 mM $MgSO_4$ and incubated for 45 minutes at 30°C. 100 μL of this mixture was plated onto LB + kanamycin plates to select for kanamycin resistant phage lysogens. All lysogens created were validated additionally with primers across the attR site.

Generation of Keio-derivative Strains

Specific *E. coli* BW25113 derivative strains, Δ*phoP*, Δ*gadB*, Δ*recA* and Δ*rcsA* from the Keio collection of single gene knockouts (Baba et al., 2006), were used to create the lysogens used in knockout comparison experiments in Figures 3 and S4. Because λ mKate contains a kanamycin resistance marker, it was imperative to remove the kanamycin resistance marker from the Keio strains.

To remove the kanamycin cassette, Keio strains were made electrocompetent. Briefly, overnight cultures grown in LB were diluted 1:100 into a low-salt LB (Thermo Fisher Scientific, 12780052) and grown to mid-exponential phase, centrifuged for 10 minutes at 7000g, washed in ice cold ddH_20 and concentrated 4-fold. Competent cells were electroporated (as previously) with pCP20, which encodes for the recombinase flippase (FLP), grown at 30°C for 1 hour, and plated on LB Carb plates and incubated at 30°C overnight. The following day, single colonies were picked, inoculated in LB, and grown overnight at 42°C to induce recombination and loss of the temperature sensitive pCP20 plasmid. 50 μL of a 10^4 dilution were plated on an antibiotic-free LB plate and incubated overnight at 30°C. Several colonies were picked and were replica streaked onto LB, LB Carb and LB Kan plates. Kanamycin and LB plates were incubated overnight at 37°C, while carbenicillin plates were incubated at 30°C. Finally, colonies that grew only on LB and were sensitive for kanamycin and carbenicillin were grown up in 3 mL LB at 37°C. These colonies were validated for the kanamycin removal by PCR reactions across the deleted gene and size was compared to original Keio strains and WT BW25113 (See Table S1B for validation primer sets). We also validated specifically the lack of functionality of the Δ*recA* mutant by treating lysogens with the prophage inducer, mitomycin C, and observed a 1.5-fold increase in phage induction frequency with WT but a slight decrease with Δ*recA* (Figure S4H).

Growth Curves

For all growth curve experiments, 96-well polystyrene plates (VWR, 655161) were used and sealed with a Excel Scientific SealPlate® that was custom laser cut to include small holes in every well. Technical triplicates of each strain were grown and were averaged in the final analysis. Plates were grown on a Biotek Epoch 2 Microplate Reader at 37°C, and OD600 reading was taken every 10 minutes for 24 hours, with linear and orbital shaking between the time points.

For λ mKate infectivity comparison, we used the previously described protocol from Maynard et al., 2010 (See Figure S1G). Overnight bacterial cultures of BW25113 were grown in 2 mL of NB at 37°C for 16 hours and were back-diluted the following morning 1:100 (roughly to OD600 = 0.02) in 2 mL fresh NB medium. The cultures were grown for 3 hours (roughly until OD600 = 0.4) and were diluted to OD600=0.1 in NB. In 200 μL final volume in polysterene plates, 15 μL of OD600=0.1 *E. coli* were grown with 15 uL of phage λ variants (10^4 plaque forming units (PFU)/mL), for a final MOI of $2x10^{-4}$. In Python, growth curves were plotted, and lysis timing was extracted from the time of peak OD within the first 8 hours of growth. Re-lysogenization time was extracted from the time point where the first derivative of growth (OD600) went above 0, for more than 3 consecutive time points.

For the lysogen and non-lysogen growth comparison (See Figure S2I), overnight bacterial cultures were grown in LB in appropriate antibiotics at 37°C for 16 hours and were back-diluted the following morning to OD600 = 0.02 in fresh medium. Cultures were grown until OD600 = 0.2 and back-diluted into polystyrene plates to OD600 = 0.02 in 200 μL of LB. The growth curves were analyzed in Python, and the growth rate was measured from the slope of [ln(OD600) / hour] from a linear regression across time points 2.865 to 5 hours during mid-exponential phase growth.

Time-Lapse Microscopy – Macrophage Infection

One day prior to imaging, RAW264.7-H2B-miRFP670 cells were seeded at 1.5 x 10^4 cells/well on a 2 μg/mL fibronectin-coated (Sigma, F0895) 96-well glass imaging plate (Fisher Scientific, 164588) in DMEM with 10% FBS and 2 mM L-glutamine. For all infection experiments, *E. coli* from overnight LB cultures, supplemented with the appropriate antibiotics, were back-diluted into fresh LB and grown to mid-exponential phase (OD600=0.4). All *E. coli* strains were grown at 37°C, except the *cI857* lysogen, which was grown at 30°C. For experiments using *cI857*, *E. coli* were heat shocked at 42°C for 15 minutes prior to infection. Bacteria were washed with PBS and resuspended at the appropriate concentration to achieve MOI 10 for the live-cell experiments, and at MOI 30 for the cross-infection experiments.

For cross-infection experiments, the temperature sensitive *cI857* lysogen was used to maximize the chances of observing the rare event. In contrast, the λ mKate (*cI* WT) lysogen, which induces once intracellular, reaches a maximum of ~20% of infected macrophages containing inducing lysogens by 21 hours (Figure 2E), whereas the *cI857* lysogen reaches a maximum of 55% of infected macrophages by 3 hours post-infection (Figure S4I).

RAW264.7 cells were infected with 5 μL of a single bacterial strain or 5 μL of a 1:1 mixture of recipient/donor strains for the cross-infection. Plates were centrifuged at 200g, 34°C for 15 minutes, and incubated at 37°C for 1 hour for live-cell experiments and 30 minutes for cross-infection. Note for the cross-infection experiments, the incubation time was optimized to be shorter to avoid missing the induction time window for the *cI857* lysogen. Cells were then washed two-three times with IM supplemented with 10 μg/mL gentamicin (Thermo-Fisher, 10687), and finally 100 μL IM/Gentamicin were added to each well. The plates were sealed with an AeraSeal, and the cells were immediately imaged.

A Nikon Eclipse Ti fluorescence microscope, encased in an environmental chamber maintained at 37°C along with 5% CO_2 was used for live-cell microscopy. The microscope was controlled by Micromanager. Images were taken at 1 hour intervals with a 20x/0.75 numerical aperture objective with 2x2 binning for single strain infections or at 11 minute intervals with 40x/0.95 numerical aperture objective + 1.5x tube lens and 2x2 binning for the cross-infection. All images were acquired on an Andor Neo 5.5 sCMOS camera. To avoid toxicity due to imaging of the mCerulean3, we also used a Neutral Density Filter (ND)-60 setting to dampen the intensity of light so that we could achieve 11 minute interval imaging.

Agar Pad Microscopy

For all time-course agar pad experiments, 1 μL of each strain concentrated to OD600=0.2 was spotted onto individual M9 glucose, 1% agarose (Low-EEO/Multi-Purpose/Molecular Biology Grade, Fisher Scientific) agar pads. At least 2 images/pad were taken at every 10 minute intervals. For single time-point agar pad experiments, *E. coli* were spotted at OD600=0.4. Pads were prepared according to Skinner et al., 2013. Pads were transferred to Labtek Chambered Coverglass (1 well, Fisher Scientific) and were imaged at 40x/0.95 numerical aperture objective + 1.5x tube lens with 2x2 binning, at 37°C.

Plaque Assay in Conditioned Media

One day before infection, RAW264.7 cells were seeded at 10^6 cells/well into 2 mL DMEM in 6-well plates and allowed to settle overnight at 37°C. MG1655 mCerulean3 non-lysogen was grown overnight in 3 mL LB at 37°C. The next day, the culture was back-diluted into 3 mL LB and grown to exponential phase (OD600=0.4). 1 mL of culture was centrifuged at 10000g, 24°C for 2 minutes, washed once with PBS (Life Technologies, 10010049), and resuspended in the appropriate volume of PBS to achieve MOI 10.

Prior to infection, RAW264.7 cells were washed twice with imaging medium, IM, and suspended in 2 mL fresh IM. 100 μL bacteria were applied to the cells. Plates were centrifuged at 200g, 34°C for 15 minutes and incubated at 37°C for 1 hour. Some wells were left uninfected in IM, some wells were left uninfected in IM with gentamicin and finally, some were infected with non-lysogen in gentamicin containing IM. Cells were washed twice with IM with gentamicin and incubated at 37°C for 16 hours. The following

day conditioned media from each treatment was collected, filter sterilized and utilized as growth medium for spontaneous induction plaque assays.

MG1655 λ mKate lysogens were grown overnight in 3 mL LB at 37°C the night before conditioned media was collected. The next day, the strain was diluted and grown to mid-exponential phase in 3 mL E-LB. *E. coli* were washed with PBS and resuspended in 3 mL of different conditioned and non-conditioned medias: LB, LB + gentamicin, IM, IM + gentamicin, IM from uninfected cells, IM from uninfected cells grown with gentamicin and finally IM from non-lysogen infected cells (See Figure S2H). Cultures were grown for 1.5 hours at 37°C in the various medias. 100-μL cells were combined with 100 μL MG1655/pUC19 plating cells and mixed with 3 mL TB soft (0.7%) agar. The cell/agar mixture was plated on TB carb plates and incubated overnight at 30°C. The Colony Forming Units (CFU) were estimated from OD600 in the different media conditions, grown for 1.5 hours, assuming OD600=2.0 is 10^9 cells/mL. Following 16 hours incubation, the number of plaque forming units (PFU) was determined to quantify the PFU/CFU ratio.

Image Processing – Segmentation and Tracking

All live-cell imaging data was analyzed using CellTK in Python (Kudo et al., 2018, https://github.com/CovertLab/CellTK). All fluorescent channels were background subtracted (Figure S3A) and the outer edges (~40% of the image) were cropped out to avoid uneven illumination around the edges of the frames due to imperfect background subtraction. Nuclear images, labeled with H2B-miRFP670, were segmented by constant thresholding of the Laplacian of Gaussian of the image followed by an adaptation of the multisnakes algorithm to round out the nuclei. Tracking of cells throughout the time course was done by using the linear assignment problem (LAP) along with watershed separation and the nearest neighbor algorithm for cells that were not detected primarily by LAP. We chose to use 1-hour time points so that we could image many different strains and growth conditions at once in one 96-well plate with at least 3 wells per strain. Furthermore, we are able to retain ~20% of the total cells post-tracking and filtering, which across 9 fields of view per condition per experiment yield ~500+ cells. After nuclei were tracked, masks of the cytoplasm were generated by using a probability map generated by CellUNet (https://github.com/CovertLab/cellunet). Briefly, we used a U-Net based deep learning architecture (Ronneberger et al., 2015), derived from Anne Carpenter (https://github.com/carpenterlab/unet4nuclei) and from DeepCell (Van Valen et al., 2016) to train a model of the cytoplasm from several labeled DIC images of thousands of macrophages, by using the train.py script with the following settings: steps – 500, epochs – 50, batches – 20, weights for loss function (1,5,1). We used this model to generate a probability map for the cytoplasm for each DIC image. Then, we iteratively extended the nuclear mask into a cytoplasm mask for each cell using the probability mask and the propagate multisnakes algorithm. We next used the cytoplasm mask to detect bacteria associated with each cell. Briefly, the bacterial channel images were preprocessed with a background subtraction wavelet method and segmented with a high-pass filter and associated with the closest cytoplasm within 25 pixels (adapted from Lane et al., 2019). Bacteria overlapping multiple cytoplasms were distributed to the cytoplasms overlapping the most bacterial pixels. We also associated a phage-positive bacterial mask with each cell by applying background subtraction wavelet to the phage mKate2 channel images, applying a constant threshold and associating only phage masks that overlapped bacterial masks with the closest cytoplasm. Thus, each cell for the time series contained a nuclear, cytoplasm, bacterial and phage mask (Figure S3A).

Next, covertrace (https://github.com/CovertLab/covertrace) was used to filter the cell traces for those that tracked well and reliably contained bacteria, using the following heuristics:

(1) The cell is present consistently at least the first 20 hours
(2) The cell is healthy (nuclear area or intensity doesn't get too small or high)
(3) The cell is reliably well tracked (no large jump in nuclear area or mean intensity between time points)
(4) Both daughter cells are connected, if the cell divides, and both traces are kept
(5) The cell contains bacteria for at least the first 3 hours (typically don't clear much before then) or first 15 hours (for clearance-adjusted analysis in Figures 3Bii and 3Cii)

Example filtered time-series traces from one field of view are shown for bacteria (Figure S3B) and phage (Figure S3C). Furthermore, we validated that the tracking filtering is non-biased and that bacterial clearance looks similar before and after filtering the time series traces (Figure S3D). Example CellTK input files and covertrace analysis filtering scripts are deposited at https://doi.org/10.17632/f5jpffyhmg.1.

For the clearance analysis in Figure 2G, at each time point, cells that were tracked well and contained bacteria for at least the first 3 hours of infection were considered. At each time point, a cell was considered to be cleared of bacteria if it had a mean intensity under the bacterial mask of less than 100, as determined from uninfected control cells, for the current time point along with the following 2 hours of time points.

Phage-Positive Bacteria-Tracking Analysis

We set out to quantify and compare the rate of prophage induction across different bacterial strains and growth conditions without introducing bias due to various macrophage infection capabilities of our bacterial strains. The metric of comparison we use in Figure 3B shows the cumulative fraction of phage-inducing bacterial-infected macrophages. We defined a macrophage as phage-positive if it was bacteria positive (contained bacteria for at least the first 3 consecutive hours post-infection) and contained a phage mask with mean intensity above a threshold (~1000 – 1200, determined by TRITC channel background in non-lysogen images, on a per experiment basis) for at least 2 consecutive frames (2 hours). See traces in Figure S3C as examples of phage-positive single cell

traces. These are generated from the mean intensity under the cytoplasm-associated phage mask. Macrophages that had multiple phage-induction events were counted only once in the sum, due to lack of granularity in time points to be able to separate induction events from each other. For each experiment per each condition (i.e. BW25113 WT), across all fields of view, the cumulative sum of phage-positive cells (from 8-9 fields of view across 3 wells), was determined for all infected nuclei tracked. This sum was divided by the number of infected macrophages at T = 3 hours. The cumulative fraction over time was then normalized to 0 at T=3. The same analysis was done for the non-lysogen strain for each condition to validate that the phage mask is specific to real phage signal. This metric was an appropriate way to track the accumulation of phage induction while bacteria are inside macrophages over time, without confounding factors such as a changing denominator of the fraction over time due to loss of bacteria at different rates of phage lysis.

Bounds Analysis for Bacterial Prophage Induction Frequency inside Macrophages

1. Assume for all infected macrophages analyzed, m, that at multiplicity of infection 10, each is maximally infected with 10 bacteria. (On average, based on the distribution in Figure S2E, we observed 2.4 bacteria/macrophage).
2. The maximum total number of bacteria present within infected macrophages is $10m$.
3. At worst, in macrophages with a phage induction event, 1 in 10 bacteria induces prophage, and at best, 10 in 10 bacteria induce prophage. (On average, based on the distribution in Figure S2F, we observed 2.1 bacteria/macrophage inducing phage).
4. At the time point where the most macrophages in the infected population experience induction, 21 hours, on average, 22% of macrophages have at least 1 bacterium inducing prophage (Based on Figure 2E).
5. Thus, the maximum frequency of bacterial prophage induction inside macrophages is the maximum number of infecting bacteria inducing phage divided by the number of infecting bacteria:

$$\frac{m(macs) \times 0.22 \times 10\left(\frac{bacs}{mac}\right) \times \frac{10}{10}(bacs\ inducing\ phage)}{10\,m} = 0.22$$

6. Thus, the minimum frequency of bacterial prophage induction inside macrophages is the minimum number of infecting bacteria inducing phage divided by the number of infecting bacteria:

$$\frac{m(macs) \times 0.22 \times 10\left(\frac{bacs}{mac}\right) \times \frac{1}{10}(bacs\ inducing\ phage)}{10\,m} = 0.022$$

Bacterial Image Analysis

All fluorescent images from agar pad experiments were background subtracted and the phase image was used to segment bacterial cells. Briefly, we trained a U-Net neural network (https://github.com/CovertLab/cellunet/) on thousands of manually curated bacterial cells. The weights that resulted from training were then used as input to the CellTK function, deep_unet, along with the phase images. The interior probabilities that were returned were thresholded at 0.3 to form bacterial masks, were opened up with watershed_labels (REG = 20) and any objects less than 6 pixels were removed. The mean intensity under bacterial masks was calculated in the relevant fluorescent channel. For all frequency of induction calculations, the phage-positive bacteria with a mean fluorescence under bacterial mask of 100 above background were enumerated and divided by total bacterial objects detected to give a fraction of inducing bacteria.

For the sensitivity analysis (Figure S1C), lysing bacteria were manually counted from two frames per experiment across n = 3 independent experiments containing > 60 lysing bacteria each. Hits were counted as bacteria that had mean phage reporter signal > 1.5x over background.

Image Analysis for Cross-Infection

The cross-infection images were analyzed manually using FIJI. Across three independent experiments, composite videos from 324 fields of view were generated of phase, mCerulean3 (Donor bacterium constitutive fluorescence), mClover (Recipient bacterium constitutive fluorescence) and mKate2 (phage lysis reporter). Each time point throughout the composite movie was carefully analyzed, as each field of view exhibited different infection patterns. The following heuristics were used to identify examples of cross-infection: (1) Only macrophages that contained both the recipient and donor bacteria at the beginning of the infection were considered for analysis. (2) After donor bacteria were lysed, attention was paid to the recipient bacteria to observe whether mKate2 signal appears and overlaps with the mClover. All mCerulean3 bacteria within a macrophage were lysed in most cross-infection samples by the time of secondary infection of mClover bacteria. (3) The cells were tracked manually by drawing a bounding box around

the cell throughout the entire time course. Maximum intensity values for mCerulean3, mClover and mKate2 channels at each time point were determined by utilizing the "Analyze" function in FIJI with the bounding box. In the case of a donor bacterium not yet being cleared by the time of recipient bacteria infection, a bacteria and phage specific mask was drawn around the recipient cell in which the maximum mKate2 and mCerulean3 pixel intensities were extracted. Traces were normalized between 0 and 1 for each example cell and were plotted in Python. An example mKate2 and mCerulean3 trace is shown in Figure 4C. For the peak analysis, the traces were preprocessed by smoothening the data with a Savitsky-Golay filter of window length 5 and polynomial order 2 and then convolving with a scaled hanning window of length 11. Peaks were extracted from the processed traces using the Python Scipy function find_peaks with the parameters (height=0.05, distance = 10). Control cells were chosen at random and were those where the macrophage was infected with both strains of bacteria at T=0 but no cross-infection occurred. These cells were analyzed similarly, and mCerulean3 signal was measured from a bounding box across the whole cell. Note, each trace analyzed as in Figure 4C is not derived from one bacterium but all bacteria across the entire cell. Therefore, we cannot exactly determine how many bacteria lyse and contribute to any given phage signal. We reasoned that since typically multiple lysogens and non-lysogens under the bacterial mask become infected with phage, any differences in phage signal due to differences in bacterial number should average out. All original cropped composites of 22 positive example cells are deposited at https://doi.org/10.17632/f5jpffyhmg.1.

The traces in Figure S4I are from performing CellTK analysis as in STAR Methods, "Image Processing – Segmentation and Tracking", however without tracking the nuclei and only detecting a bacterial mask associated with the lysogen-only infected cells. For Figure S4I, the percent of macrophages with any detected mCerulean3 bacteria expressing the mKate2 lysis reporter was calculated at each time point independently across all cells analyzed.

QUANTIFICATION AND STATISTICAL ANALYSIS

All data are presented as the mean ± s.e.m. unless otherwise indicated in the figure legends or raw data points are displayed directly. The number of technical and independent biological replicates for each experiment is indicated in the figure legends or STAR Methods. No blinding or randomization was used in these experiments. All live-cell microscopy and agar pad microscopy data were analyzed as according to STAR Methods, and any modifications made to the protocol are indicated in the figure legends. All statistical significance tests were carried out in Python, and a two-sided student's t-test was used.

DATA AND CODE AVAILABILITY

Software for neural network training, cellunet, is located at https://github.com/CovertLab/cellunet/. All other software used is described in STAR Methods. The raw data including all the image files are too large to upload to existing public repositories. We deposited all single cell example composite images from Figure 4 and an example of the full image analysis workflow to Mendeley Data: https://dx.doi.org/10.17632/f5jpffyhmg.1.